Stieltjesweg 1
2628 CK Delft
Postbus 155
2600 AD Delft

www.tno.nl

T +31 88 866 20 00

**TNO-rapport**

**TNO 2020 R10850A**

# Typologie-gebaseerde beoordeling van de veiligheid bij aardbevingen in Groningen - Uitwerking van typologiegroep METSELWERK-D

| | |
|---|---|
| Datum | 12 januari 2022 |
| Auteur(s) | Dr.Ir. C.P.W.Geurts, Prof.Dr.Ir. R.D.J.M. Steenbergen, Ir. D. Moretti, Ir. J.P. Pruiksma, Ir.Ing. M. Steins-Zwanenburg |
| Exemplaarnummer | |
| Oplage | |
| Aantal pagina's | 77 (incl. bijlagen) |
| Aantal bijlagen | 3 |
| Opdrachtgever | Ministerie van EZK<br>t.a.v. de heer P.A.C.M. Brouwers MSc. |
| Projectnaam | Typologie aanpak |
| Projectnummer | 060.39973/01.01 |

# Samenvatting

Dit rapport beschrijft de uitwerking van de typologie gebaseerde beoordeling zoals omschreven in het hoofdrapport [TNO, 2021a] voor de typologiegroep METSELWERK-D. Deze typologiegroep bestaat uit gebouwen met 3 tot 5 bouwlagen met een draagconstructie van metselwerk. Het materiaal van de vloer van de tweede en hogere bouwlaag is van beton.

Dit rapport beschrijft de totstandkoming van het sterkte- en gevolgmodel voor de typologiegroep METSELWERK-D, in de vorm van de kwetsbaarheidskromme, de parameters die deze kromme beschrijven en de parameters voor het gevolgmodel.

Er wordt voor de beoordeling geen onderscheid gemaakt in onderliggende typologieën. Voor de typologiegroep wordt gebruik gemaakt van een veilige keuze ten aanzien van het berekend risico. De naam van de typologiegroep en typologie is derhalve dezelfde.

De keuze voor het sterkte- en gevolgmodel is gebaseerd op referentiegebouwen waarvoor uitgebreide berekeningen beschikbaar zijn. Er is ervoor gekozen om het gebouw met het hoogste berekende risico als uitgangspunt te kiezen voor de hele typologie.
In het rapport wordt aannemelijk gemaakt dat deze keuze voldoende veilig is voor meerdere representatief geachte gebouwen uit deze typologie. Op basis daarvan is ervoor gekozen het gekozen sterkte- en gevolgmodel te gebruiken voor de berekening van het risico voor de hele typologiegroep.

De kwetsbaarheidskromme is toegepast in een berekening met de TNO modelketen. Deze berekening resulteert in een vlekkenkaart waarin is aangegeven waar de typologiegroep METSELWERK-D wel, dan wel niet voldoet aan de Meijdam norm.

.

# Inhoudsopgave

**1 Inleiding ..... 4**

**2 Omschrijving typologiegroep ..... 5**

**3 Overzicht van gemodelleerde gebouwen ..... 7**
3.1 Algemeen ..... 7
3.2 Eigenschappen van de gebruikte referentiegebouwen ..... 8
3.3 Relatie met gebouwvoorraad in Groningen ..... 9
3.4 Uitgevoerde berekeningen voor de referentiegebouwen ..... 9
3.5 Faalmechanismes van de referentiegebouwen ..... 10
3.6 Gebouwen gebruikt in aanvullende analyses ..... 11

**4 Afleiding kwetsbaarheidsmodel en gevolgmodel ..... 14**
4.1 Beschikbare informatie voor het kwetsbaarheidsmodel ..... 14
4.2 Afleiding kwetsbaarheidsmodel voor de referentiegebouwen ..... 14
4.3 Mediane seismische capaciteit voor de typologie ..... 15
4.4 Gebouw tot gebouw variatie voor de typologie ..... 16
4.5 Modelonzekerheid ..... 17
4.6 Gevolgmodel ..... 17
4.7 Nadere beschouwing parameterkeuzes METSELWERK D. ..... 18

**5 Sterkteparameters in de TNO modelketen-berekening voor METSELWERK-D ..... 20**

**6 Controles ..... 21**
6.1 NLTH berekeningen ..... 21
6.2 Gebouw tot gebouw variabiliteit ..... 22
6.3 Vergelijking met NPR berekeningen ..... 22

**7 Vlekkenkaart voor METSELWERK-D ..... 23**

**8 Referenties ..... 24**

**9 Ondertekening ..... 27**

**Bijlage(n)**
A Vergelijking met beschikbare NPR berekeningen
B Ligging referentiegebouwen in Groningse gebouwenpopulatie
C Summary of the material received from NCG

# 1 Inleiding

De gaswinning in Groningen leidt tot het ontstaan van ondiepe aardbevingen. Hoewel deze aardbevingen relatief licht zijn (in termen van Magnitudes op de Richterschaal), zijn de effecten aan het aardoppervlak door de relatief ondiepe locatie (3 km) van het hypocentrum aanzienlijk. Er is een grote opgave om het veiligheidsniveau voor de bewoners van Groningen te borgen.

In TNO Rapport 2020 R10628/A [TNO 2021a] is een uniforme aanpak beschreven voor de beoordeling van de gebouwen in Groningen. Deze aanpak is erop gebaseerd dat gebouwen worden ingedeeld in een typologie. Per typologie worden de seismische kenmerken bepaald, rekening houdend met de variaties tussen gebouwen binnen die typologie. Op basis van deze kenmerken kan snel voor een gehele typologie worden bepaald of en zo ja waar deze voldoet aan de norm. De norm die bij de veiligheidsbeoordeling wordt gehanteerd is de Meijdam norm (het Individueel Risico per jaar moet gelijk aan of kleiner zijn dan $10^{-5}$). TNO Rapport 2020 R10628/A zal vanaf nu worden aangeduid als het hoofdrapport [TNO, 2021a].

In dit rapport wordt deze aanpak ingevuld voor de typologiegroep METSELWERK-D. Voor de indeling van gebouwen in typologieën en typologiegroepen inclusief de bijbehorende kenmerken wordt verwezen naar het hoofdrapport [TNO, 2021a]. Het voorliggende rapport moet in samenhang met het hoofdrapport beschouwd worden.

Dit rapport is als volgt opgebouwd: Hoofdstuk 2 geeft kort een omschrijving van de typologiegroep. In hoofdstuk 3 wordt de informatie die gebruikt is om het sterkte-model voor de typologie af te leiden beschreven. Hoofdstuk 4 gaat nader in op de afleiding van het kwetsbaarheids- en gevolgmodel. Hoofdstuk 5 geeft het overzicht van de parameters die afgeleid zijn ten behoeve van het berekenen van het risico met de TNO Modelketen. Hoofdstuk 6 beschrijft de uitwerking van de door ACVG gevraagde controles voor deze typologie. In hoofdstuk 7 is de vlekkenkaart die van toepassing is voor de typologiegroep METSELWERK-D gegeven.

# 2 Omschrijving typologiegroep

De typologiegroep METSELWERK-D omvat de gebouwen met drie tot en met vijf bouwlagen, die hun stabiliteit ontlenen uit een (ongewapend) metselwerk draagconstructie. Deze typologiegroep omvat voornamelijk gebouwen met appartementen. Dit betekent dat per gebouw doorgaans meerdere adressen aanwezig zijn. Typische gebouwen in deze typologiegroep zijn portiekflats en woongebouwen met beneden- en bovenwoningen.

De stabiliteit in de dwarsrichting van het gebouw (de sterke richting) wordt verzorgd door metselwerk wanden (de dragende wanden die individuele adressen scheiden). De stabiliteit in de langsrichting (de zwakke richting) wordt verzorgd door metselwerk in de langsgevel en de aanwezigheid van binnenwanden, eventueel aangevuld met bijdragen uit gekoppelde betonnen vloeren, bijdragen van de vloer-wand verbindingen en de koppeling tussen vloeren en het dakvlak. Het dak van de gebouwen bestaat in de praktijk uit een betonnen of houten platdakconstructie of een houten kapconstructie met een tweezijdig hellend dak.

Uit de resultaten van de analyses in dit rapport volgt dat een verdere onderverdeling van de typologiegroep in typologieën niet nodig wordt geacht voor de risicobeoordeling. Dit wordt naar aanleiding van de ontwikkeling van het kwetsbaarheids- en gevolgmodel in hoofdstuk 4 nader toegelicht.

In Figuur 1 is ter illustratie een voorbeeld gegeven van een gebouw dat tot de typologiegroep METSELWERK-D behoort.

Figuur 1: Voorbeeld van een gebouw van typologiegroep METSELWERK-D (bron Google Street View)

In Tabel 1 is de omschrijving van de typologiegroep aan de hand van de toedelingskenmerken gegeven. Deze tabel is een update van pagina B19 van het toedelingsrapport [TNO, 2021b].

| TYPOLOGIEGROEP<br>omschrijving | **METSELWERK-D**<br>Meerlaagse bouw (appartementen) |
|---|---|
| TYPOLOGIE | **METSELWERK-D** |
| NADERE OMSCHRIJVING | Meerlaagse bouw, draagconstructie uit metselwerk |
| **INSPECTIEGEGEVENS** | |
| MATERIAAL CONSTRUCTIE (richting X) | Metselwerk (stapelbouw) |
| CONSTRUCTIESYSTEEM (richting X) | Schijfwerking wanden |
| MATERIAAL CONSTRUCTIE (richting Y) | Metselwerk (stapelbouw) |
| CONSTRUCTIESYSTEEM (richting Y) | Schijfwerking wanden (gevel en eventuele stabiliserende binnenwanden) met eventueel doorlopende gekoppelde betonnen vloeren. |
| AANTAL BOUWLAGEN | 3 tot en met 5 |
| VRIJSTAAND of GESCHAKELD (indien geschakeld, wel of niet seriematig) | Geschakeld, seriematig |
| MATERIAAL VLOER | Beton |
| OPBOUW METSELWERK IN GEVEL | Spouwmuur |

Tabel 1: Overzicht omschrijving typologie(groep) METSELWERK-D; deze tabel is de update van de tabel uit [TNO, 2021b, pg B19]

# 3 Overzicht van gemodelleerde gebouwen

## 3.1 Algemeen

Voor de uitwerking van typologieën wordt gebruik gemaakt van beschikbare gekalibreerde niet-lineaire tijddomein berekeningen (NLTH, *Non Linear Time History*). Voor de typologiegroep METSELWERK-D zijn bruikbare berekenings-resultaten voor twee gebouwen beschikbaar waarbij state-of-the art NLTH berekeningen uitgevoerd zijn. Deze gebouwen zijn in opdracht van NAM door Arup doorgerekend, en zijn aangeduid als Schuitenzandflat en Koeriersterweg [Arup (2017a,2019a,2020a)]. Een afbeelding van de 2 gebruikte referentiegebouwen is weergegeven in Figuur 2.

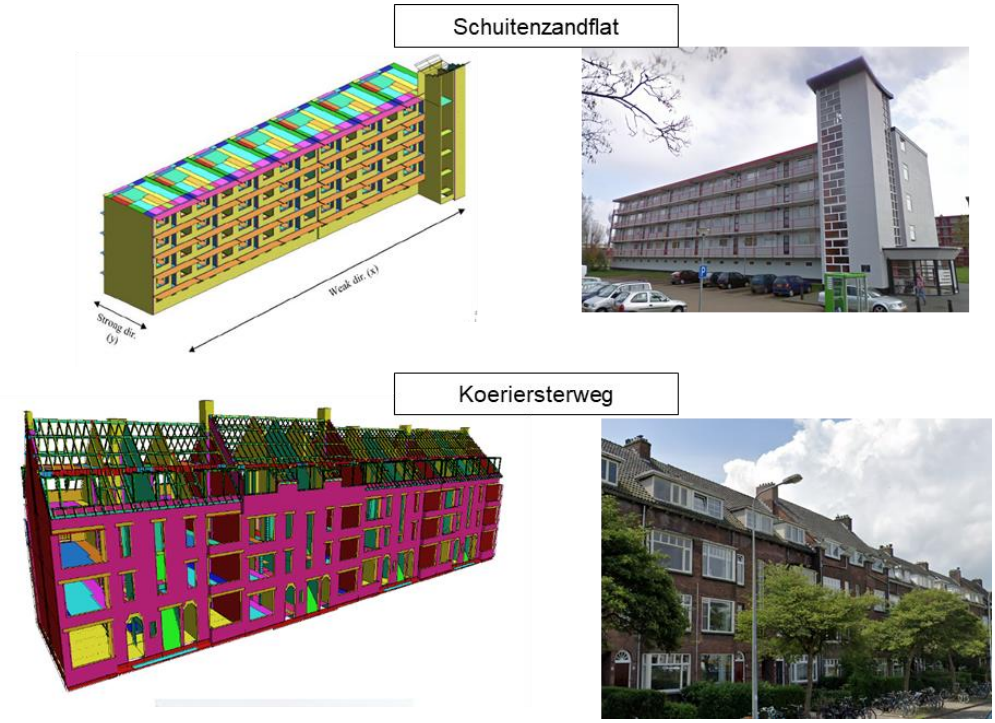


Figuur 2: Illustratie van de referentiegebouwen

De berekeningsresultaten van deze gebouwen zijn door Eucentre in achtereenvolgende versies van het *fragility and consequence model* gebruikt voor het afleiden van zogenaamde *fragility functions*, ofwel kwetsbaarheidskrommen [Crowley et al, 2017; Crowley et al, 2019; Crowley et al, 2020]. De informatie uit deze berekenings-resultaten is in dit rapport als basis gebruikt voor de bepaling van de parameters voor de typologiegroep METSELWERK-D. Door TNO zijn deze beschikbare resultaten geanalyseerd en er zijn eigen keuzes gemaakt voor de te hanteren parameterwaarden ten behoeve van de definitieve berekeningen van de typologieën.

De twee referentiegebouwen vormen een smalle basis voor het vastleggen van de parameterwaarden. Nagegaan is daarom welke additionele informatie beschikbaar en bruikbaar is om te komen tot de definitieve keuzes voor de parameterwaarden.

Er is daarvoor gebruik gemaakt van reeds beschikbare berekeningsresultaten aan de hand van NPR 9998, en een afstudeerrapport van de TU Delft. Deze worden in paragraaf 3.6 nader omschreven.

### 3.2 Eigenschappen van de gebruikte referentiegebouwen

De gebouwen Schuitenzandflat en Koeriersterweg zijn door Eucentre gebruikt als referentiegebouw voor de uitwerking van sterktemodellen van twee kwetsbaarheidsklasses, zie voor de beschrijving daarvan Tabel 2.

Tabel 2: Relatie tussen gebruikte referentiegebouwen en Eucentre rapporten

| **Eucentre versie** | **Referentiegebouw** | **Kwetsbaarheidsklasse** | **Omschrijving** |
|---|---|---|---|
| V7 [2020] | Koeriersterweg | URM3M_U | *Unreinforced masonry 3+ storey aggregate unit with cavity walls and concrete floor* |
| V7 [2020] | Schuitenzandflat | URM3M_B | *Unreinforced masonry 3+ storey block unit with cavity walls and concrete floor.* |

De belangrijkste eigenschappen van de genoemde referentiegebouwen zijn in Tabel 3 samengevat.

Tabel 3: Overzicht van relevante eigenschappen per referentiegebouw

| **Eigenschap** | **Referentiegebouw** | |
|---|---|---|
| | **Schuitenzandflat (S-Flat)** | **Koeriersterweg (K-Flat)** |
| Eucentre kwetsbaarheidsklasse | URM3M_B | URM3M_U |
| Aantal verdiepingen | 5 | 4 met zolder onder de kap |
| Hoogte | 13,70 m | 14 m |
| Binnenwanden | Metselwerk (100 mm kalkzandsteen) | Metselwerk (110 mm dik) |
| Dragende en woning-scheidende wanden | Metselwerk (220mm) | Metselwerk (220mm) |
| Vloeren | Gewapend beton | Gewapend beton |
| Dak | Beton (vloer) | Houten kap |

De relevante eigenschappen van beide kwetsbaarheidsklasses passen in de omschrijving van typologiegroep METSELWERK-D. Beide referentiegebouwen worden daarom geanalyseerd als basis voor METSELWERK-D. Het verschil in gedrag tussen beide gebouwen wordt in hoofdstuk 4 geanalyseerd. Op basis van de behandeling van de rekenresultaten wordt vervolgens gemotiveerd of een splitsing in twee typologieën mogelijk dan wel wenselijk is.

## 3.3 Relatie met gebouwvoorraad in Groningen

Het is van belang te weten in hoeverre op geometrisch én op constructief niveau de gebruikte referentiegebouwen representatief zijn voor de Groningse gebouwvoorraad binnen de typologiegroep METSELWERK-D. Hierover is de beschikbare informatie verzameld en geanalyseerd.

1. In Bijlage B wordt de beschikbare informatie beschreven en wordt getoond dat met betrekking tot de geometrische eigenschappen de gebruikte referentiegebouwen representatief zijn voor de aanwezige gebouwvoorraad voor de typologiegroep METSELWERK-D. De hoeveelheid informatie die hiervoor beschikbaar is, is echter beperkt.
2. Met betrekking tot de representativiteit op constructief niveau is er geen directe informatie beschikbaar.

Bovenstaande punten zijn reden om extra informatie mee te nemen vanuit de gebouwen waarvoor door de NCG NPR9998 berekeningen beschikbaar zijn gesteld (zie paragraaf 3.6 voor het overzicht). Deze gebouwen worden gezien als een representatieve doorsnede voor METSELWERK-D. In hoofdstuk 4 wordt beschreven in hoeverre het seismisch gedrag van deze gebouwen past binnen de keuzes gemaakt voor het sterktemodel. Uit die beschrijving volgt dat dit gedrag goed overeenkomt. Dit wijst erop dat de gemaakte keuzes op basis van de referentiegebouwen voldoende de variaties van gebouwen in Groningen voor METSELWERK-D afdekken.

## 3.4 Uitgevoerde berekeningen voor de referentiegebouwen

Berekeningen (NLTH) zijn uitgevoerd door Arup in LS-Dyna. Voor de modellering van het metselwerk heeft Arup een nieuw materiaalmodel ontwikkeld; de beschrijving en validatie daarvan is gerapporteerd in het ‘LS-DYNA Validation Booklet’ [Arup, 2016a]. Voor zowel in-het-vlak als uit-het-vlak gedrag van metselwerk wanden laat [Arup, 2016a] zien dat de modelmatig verkregen resultaten goed overeenstemmen met experimenteel verkregen resultaten. Om die reden wordt het gebruikte model door TNO als state-of-the-art en voldoende representatief gezien. In [Arup 2020a] is een verdere verbetering aan dit materiaalmodel beschreven, voor details hieromtrent zie Bijlage A.5. De berekeningen uitgevoerd met dit verbeterde materiaalmodel aan de referentiegebouwen vormen de basis voor de analyses in dit rapport.

In de berekeningen van Arup is gebruik gemaakt van ten minste 8 aardbevingssignalen die als representatief worden beschouwd voor de mogelijk optredende aardbevingsbelasting. Voor verdere omschrijving van de gebruikte materiaaleigenschappen en uitgevoerde berekeningen wordt verwezen naar de

berekeningen van Arup zoals gerapporteerd in [Arup, 2017a], [Arup, 2019a] en [Arup, 2020a].

De berekeningen zijn uitgevoerd voor beide hoofddraagrichtingen van de gebouwen. Per hoofddraagrichting zijn voor de doorgerekende aardbevingssignalen de maximale verplaatsing ter plaatse van de zolderverdieping in geval van de Koeriersterweg en ter plaatse van het dak voor de Schuitenzandflat en de maximaal optredende dwarskracht ter hoogte van de begane grond vloer (net voor falen) gerapporteerd. Per berekening is gerapporteerd wat de effecten zijn op het gebouw. Deze effecten verschillen per doorgerekend signaal van geen effect (het gebouw blijft intact), tot aan volledige instorting met per berekening bepaalde percentages volumeverlies.

## 3.5 Faalmechanismes van de referentiegebouwen

De faalmechanismes die zijn waargenomen in de uitgevoerde berekeningen met de laatste update van het metselwerkmodel (zie Arup [2020a]) zijn samengevat in Tabel 4.

Tabel 4: *Faalmechanismes voor de verschillende collapse states voor de 2 gebruikte referentiegebouwen*

| | **Faalmechanisme voor collapse state** | | |
|---|---|---|---|
| | **CS1** | **CS2** | **CS3** |
| **Schuitenzandflat** | Local connection failure of roof slab/wall,<br>OOP failure of URM internal walls on 3rd floor | N/A | Complete collapse starting from in-plane failure of first floor. |
| **Koeriersterweg** | Onset of collapse of chimneys | Overturning of URM walls in roof, roof and chimney collapse.<br>OOP failure of URM outer leaf in all units | Collapse of the attic storey likely followed by progressive collapse onto lower levels. |

De faalmechanismes voor deze beide gebouwen onderscheiden zich van elkaar: Bij het gebouw Koeriersterweg zijn de faalmechanismes gekoppeld aan de aanwezigheid van een hellend dak en een schoorsteen. Bij de Schuitenzandflat zijn de faalmechanismes gekoppeld aan zowel uit-het vlak falen van binnenwanden als in-het-vlak falen van de eerste verdieping.
In hoofdstuk 4 worden beide gebouwen afzonderlijk geanalyseerd en wordt een keuze gemotiveerd voor de aan te houden parameters voor de hele typologiegroep.

### 3.6 Gebouwen gebruikt in aanvullende analyses

In hoofdstuk 4 wordt een aanvullende beschouwing gegeven waarin gebruik gemaakt is van beschikbare berekeningen uit andere bronnen. Dit betreft de volgende gebouwen.

1: In een afstudeerrapport aan de TU Delft [Noortman, 2019] is een NLTH studie uitgevoerd in Diana voor een meerlaags appartementengebouw in de provincie Groningen. Door TNO en TU Delft is deze studie beoordeeld op kwaliteit en bruikbaarheid. De berekeningen hebben voldoende kwaliteit voor toepassing in de aanvullende beschouwingen in dit rapport.
2: Door NCG zijn de resultaten van berekeningen uitgevoerd volgens NPR9998 beschikbaar gesteld voor meerdere gebouwen die voldoen aan de typologie-kenmerken. Dit betreft berekeningen met verschillende NPR versies. Deze berekeningen zijn geanalyseerd en de informatie die geschikt is voor vergelijking met de uitkomsten van de voorgestelde eigenschappen van de typologie is gebruikt in bijlage A.

Alleen die gebouwen zijn gebruikt waarvoor NLTH dan wel NLPO berekeningen beschikbaar waren. Berekeningen met andere, gesimplificeerde, methoden zijn niet geschikt voor de beschouwing in bijlage A.

De gebouwen waarvan deze berekeningen gebruikt zijn, zijn in Tabel 5 weergegeven.

Tabel 5: Gebouwen gebruikt voor aanvullende analyses

| |
|---|
|  <br>Gebouw uit [ Noortman, 2019] |
|  ,<br>Rijksweg 107-117B |

Rijksweg 119-129B

Helling 2-6/Jachtlaan 16-18B

Georg van Saksenlaan 27-37B

Abel Eppensstraat 15-69

De Rank 7-11B

# 4 Afleiding kwetsbaarheidsmodel en gevolgmodel

Dit hoofdstuk geeft de achtergronden bij het gebruikte kwetsbaarheids- en gevolgmodel voor de typologiegroep METSELWERK-D. In het hoofdrapport [TNO, 2021a] is omschreven welke stappen worden doorlopen om deze modellen af te leiden.

Voor de bepaling van het kwetsbaarheidsmodel met een gebouw-tot-gebouw variatie binnen METSELWERK-D is het van belang te weten hoe de precieze opbouw van een gebouw binnen de grenzen van de definitie van METSELWERK-D kan variëren. Dit betreft de opbouw van de stabiliteitswanden, de gevels, verbindingen, materiaaleigenschappen, et cetera. De variatie in deze opbouw wordt in dit hoofdstuk vertaald naar de parameters voor de kwetsbaarheidscurve.

In dit hoofdstuk wordt in paragraaf 4.1 eerst beschreven welke informatie beschikbaar is met betrekking tot het kwetsbaarheidsmodel, vervolgens wordt de voor de typologie te gebruiken mediaan in de kwetsbaarheidskromme afgeleid, in paragraaf 4.4 wordt de gebouw tot gebouw spreiding vastgesteld, in paragraaf 4.5 wordt ingegaan op de modelonzekerheid en in paragraaf 4.6 wordt het gevolgmodel besproken. In paragraaf 4.7 worden de keuzes die zijn gemaakt op basis van de gebruikte referentiegebouwen geëvalueerd aan de hand van beschikbare berekeningen voor de gebouwen zoals beschreven in Tabel 5 in hoofdstuk 3.

## 4.1 Beschikbare informatie voor het kwetsbaarheidsmodel

Voor METSELWERK-D zijn berekeningsresultaten van Arup voor twee referentiegebouwen beschikbaar. De berekeningsresultaten van deze gebouwen zijn door Eucentre gebruikt voor het afleiden van de zogenaamde *fragility curve*, ook wel kwetsbaarheidskromme genoemd, in [Crowley et al, 2020]. Deze resultaten worden gebruikt voor het kwetsbaarheidsmodel voor METSELWERK-D.

## 4.2 Afleiding kwetsbaarheidsmodel voor de referentiegebouwen

In deze paragraaf wordt het kwetsbaarheidsmodel voor de twee referentiegebouwen van METSELWERK-D afgeleid.
In Tabel 4 zijn de gevonden faalmechanismen voor de 2 genoemde referentiegebouwen samengevat. In Figuur 3 zijn de backbone curves voor beide referentiegebouwen weergegeven. Het CS3 falen van Koeriersterweg betreft het instorten van de zolderverdieping, het CS3 falen van Schuitenzandflat betreft het in-het-vlak falen van de bouwlaag op de begane grond.

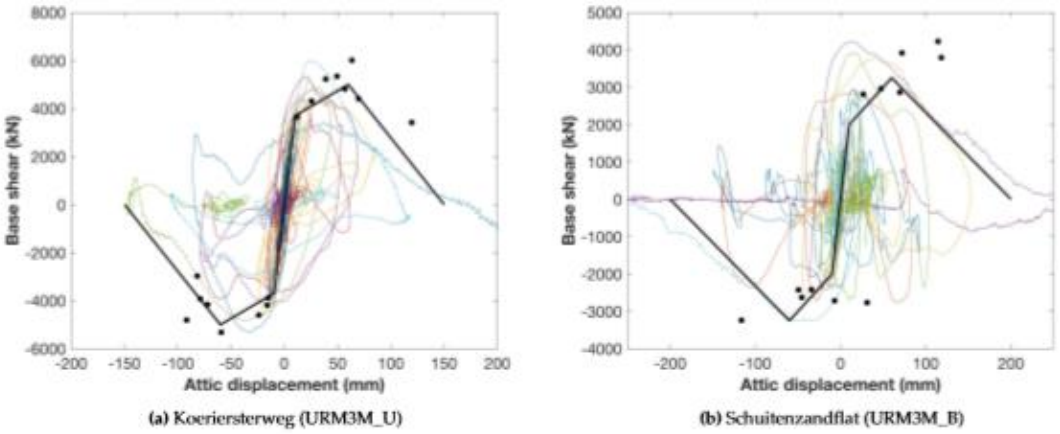


Figuur 3: Backbone curves voor de gebruikte referentiegebouwen op basis van berekeningen met de verbeterde materiaalmodellen, uit [Crowley et al, 2020]

Deze backbone curves zijn in [Crowley et al, 2020] gebruikt voor het bepalen van de kwetsbaarheidskromme inclusief de record-to-record variatie per referentie-gebouw. Hierin is uitgegaan van een schematisatie tot een één-massa-veer-systeem. Deze wijze van schematiseren is een zekere mate van versimpeling, echter het draaien van vele duizenden NLTH's voor dit doel zou te veel tijd vergen. De verschillen tussen NLTH uitkomsten en de uitkomsten van de berekeningen aan één-massa-veer-systemen worden verdisconteerd door toepassing van een mediaanshift en een vergrote onzekerheid. Hier wordt in paragraaf 4.5 nader op ingegaan.

Er zijn kwetsbaarheidskrommes voor de referentiegebouwen Koeriersterweg en Schuitenzandflat afgeleid in [Crowley et al, 2020]. Er is voor deze referentie-gebouwen afgeleid dat voor Koeriersterweg het hoogste risico wordt gevonden. In hoofdstuk 3 zijn de belangrijkste kenmerken van beide gebouwen gegeven. Er is ervoor gekozen om geen verdere onderverdeling van METSELWERK-D te maken. Er is voor gekozen voor METSELWERK-D uit te gaan van het kwetsbaarheids-model van het maatgevende gebouw in termen van risico. Dit risico is berekend aan de hand van het gevolgmodel per referentiegebouw, zoals toegelicht in 4.6, gebruikmakend van de resultaten uit [Crowley et al, 2020].
Dit berekend risico is het hoogste voor het referentiegebouw Koeriersterweg (URM3M_U). Derhalve wordt voor het kwetsbaarheids- en gevolgmodel uitgegaan van dit gebouw.

In paragraaf 4.3 wordt ingegaan op de keuze voor de mediane seismische capaciteit van deze kwetsbaarheidskromme en in paragrafen 4.4 en 4.5 wordt de parameterkeuze voor de gebouw-tot-gebouw onzekerheid en de modelonzekerheid toegelicht.

## 4.3 Mediane seismische capaciteit voor de typologie

In bijlage C.4 van het hoofdrapport [TNO, 2021a] is op basis van MDOF variatie-studies een beschouwing gehouden over de mediane seismische capaciteit. Gebruik is gemaakt van beschikbare studies [Arup 2019b, c]. In deze studies zijn

kwetsbaarheidskrommen afgeleid op basis van een volledige MDOF (NLTH) benadering waarbij voor de variaties een koppeling is gemaakt naar de Groningen Exposure Database. De beschouwingen in het hoofdrapport leveren een aanpassing van de gebruikte kwetsbaarheidskromme in de vorm van een verlaging van de mediane seismische capaciteit van 15%.
De MDOF variatie studie betrof alleen de typologieën METSELWERK 1 en 2. Dergelijke berekeningen zijn niet beschikbaar voor METSELWERK-D. Er is evenwel ervoor gekozen om de aanpassing op de kwetsbaarheidskromme ook toe te passen op METSELWERK-D. Omdat een uitgebreide MDOF-SDOF studie niet beschikbaar is voor METSELWERK-D is het niet zeker of deze correctie hier adequaat is. Er is daarom een aanvullende beschouwing gemaakt op basis van beschikbare NPR berekeningen. Hierop wordt in paragraaf 4.7 teruggekomen.

In Tabel 6 zijn de parameters gegeven voor de kwetsbaarheidskromme voor METSELWERK-D die worden gebruikt in de modelketenberekening. Deze zijn rechtstreeks gehaald uit tabel 6.3 van [Crowley et al, 2020] op basis van de uitwerking van Koeriersterweg. Deze parameters bevatten de besproken mediaanshift. De 'Upper-branch' (zwakkere branch) $b_0$ waarde uit [Crowley et al, 2020] wordt gebruikt voor de 'Middle-branch' in de modelketenberekening, zoals besproken in paragraaf 4.2.5 van het hoofdrapport [TNO, 2021a].
Voor de betekenis van deze parameters wordt verwezen naar bijlage D van het hoofdrapport [TNO, 2020].

Tabel 6: Parameters kwetsbaarheidskromme METSELWERK-D

| **Parameters kwetsbaarheidskromme** | **METSELWERK-D** |
|---|---|
| $b_0$ | -1,9877 |
| $b_1$ | 2,2622 |
| $\sigma_s$ | 1,0038 |
| DL_CS1 | 0,023 |
| DL_CS2 | 0,102 |
| DL_CS3 | 0,131 |

## 4.4 Gebouw tot gebouw variatie voor de typologie

In het hoofdrapport [TNO, 2021a] is in bijlage C.4 op basis van MDOF variatie-studies een beschouwing gehouden over de gebouw-tot-gebouw variatie van metselwerk gebouwen en een waarde van $\sigma_{BB}$=0,30 voorgesteld. De in het hoofdrapport beschouwde gebouwen betreffen alleen METSELWERK 1 en 2 gebouwen en geen METSELWERK-D gebouwen.
Voor METSELWERK-D wordt eveneens een gebouw-tot-gebouw variatie van $\sigma_{BB}$=0,30 voorgesteld. Deze keuze wordt nader gemotiveerd op basis van de volgende punten:

- Ten behoeve van de definitie van METSELWERK-D is er voor gekozen alleen (nagenoeg) rechthoekige gebouwen te beschouwen. Eventuele variaties in plattegrond zijn daarmee als uitsluitingsgrond gedefinieerd en behoeven ook niet in de gebouw tot gebouwvariatie te worden meegenomen.

- De belangrijkste faalmechanismen binnen METSELWERK-D betreffen in-het-vlak falen. Bij METSELWERK 1 en 2 betrof dit in-het-vlak én uit-het-vlak falen of combinaties daarvan. Naar verwachting is vanwege de eenduidigheid van het faalmechanisme de gebouw-tot-gebouw spreiding voor METSELWERK-D kleiner of gelijk aan die van METSELWERK 1 en 2.

- Vanwege de dikte van 200-220mm van de dragende metselwerk wanden speelt uit-het-vlak bezwijken naar verwachting geen grote rol. De spreiding die ontstaat door uit-het-vlak bezwijken is daarom minder belangrijk dan bij METSELWERK 1 en 2.

In paragraaf 4.7 wordt de keuze van $\sigma_{BB}$=0,30 nog nader geëvalueerd op basis van een vergelijking met beschikbare NPR berekeningen.

## 4.5 Modelonzekerheid

Het effect van versimpelingen in de modellering van de gebouwen wordt opgenomen in de modelonzekerheid. De waarde voor de modelonzekerheid $\beta_m$ volgt uit de waarden voor $\beta_c$ en $\beta_q$ zoals in het hoofdrapport toegelicht en deze wordt geïmplementeerd via een ‘logic tree’ zoals toegelicht in het hoofdrapport [TNO, 2021a].

Er is gekozen om voor $\beta_q$ (voor definitie zie het hoofdrapport [TNO, 2021a], bijlage D), voor METSELWERK-D, een waarde $\beta_q$=0,25 te gebruiken, omdat het SDOF model niet als ‘superior’ conform de FEMA terminologie [FEMA, 2012] kan worden gezien. Voor $\beta_c$ wordt de waarde 0,25 aangehouden, conform bijlage D van het hoofdrapport [TNO, 2021a].

De modelonzekerheid wordt verwerkt in een ‘logic tree’ met 3 takken: ‘lower’, ‘middle’ en ‘upper’. Dit leidt tot de waarden van $b_{0lower}$ en $b_{0upper}$ in onderstaande tabel. Voor achtergronden hierbij en de betekenis van deze parameters zie bijlage C.3 van het hoofdrapport [TNO, 2021a].

Tabel 7: Parameters voor de modelonzekerheid van METSELWERK-D

| **Parameters** | **METSELWERK-D** |
|---|---|
| $b_{0lower}$ | -2,5932 |
| $b_{0middle}$ | -1,9877 |
| $b_{0upper}$ | -1,3822 |
| Modelonzekerheid $\beta_m$ | 0,35 |

De waarden voor $b_{0lower}$ en $b_{0upper}$ zijn verkregen door toepassing van de modelonzekerheid op de in paragraaf 4.2 tot en met 4.4 afgeleide mediane kwetsbaarheidskromme. Zie voor de achtergronden bijlage D van het hoofdrapport [TNO, 2021a].

## 4.6 Gevolgmodel

Voor de gevolgmodellering wordt het model gebruikt zoals beschreven in bijlage D van het hoofdrapport [TNO, 2021a]. Voor de gevolgmodellering worden het model en de waarden uit [Crowley et al, 2020] als basis genomen. In dat rapport wordt

voor CS3 uitgegaan van een overlijdenskans gegeven falen van 0,42. Gegeven de wijze van instorten zoals waargenomen in de NLTH-berekeningen van de referentiegebouwen acht TNO dit een redelijke waarde.

URM3M_U (Koeriersterweg) levert gegeven instorting een groter oppervlak bedolven met puin en daarmee een grotere kans op overlijden dan URM3M_B (Schuitenzandflat). Dit levert in de uitwerking met het kwetsbaarheidsmodel een hoger berekend risico op voor URM3M_U vergeleken met URM3M_B. De klasse URM3M_U is daarom maatgevend en de bovengrens-waarden uit Tabel 6.6 van [Crowley et al, 2020] voor de klasse URM3M_U (Koeriersterweg) worden in de typologieaanpak voor METSELWERK-D gebruikt. In paragraaf 4.3 van het hoofd-rapport [TNO, 2021a] is nadere toelichting gegeven over het gebruik van deze bovengrens-waarden.

In Tabel 8 zijn de door TNO gebruikte parameters van het gevolgmodel gegeven zoals toegepast als meest waarschijnlijke schatting voor alle *collapse states*. Dit leidt tot de waarden van de overlijdenskansen zoals deze op de 'middle' branch van het gevolgmodel zijn gebruikt. Voor de 'lower' en 'upper' branch wordt verwezen naar het hoofdrapport [TNO, 2021a].

Tabel 8: Parameters voor de gevolgmodellering voor METSELWERK-D

| | |
|---|---|
| Pd_inside\|CS1 | 0,0252 |
| Pd_inside\|CS2 | 0,0395 |
| Pd_inside\|CS3 | 0,42 |
| Pd_outside\|CS1 | 0,0402 |
| Pd_outside\|CS2 | 0,063 |
| Pd_outside\|CS3 | 0,67 |

## 4.7 Nadere beschouwing parameterkeuzes METSELWERK D

In de voorgaande paragrafen zijn parameters afgeleid voor de berekening van de kwetsbaarheid van METSELWERK-D. Hierbij zijn naar analogie van de afleiding van andere typologieën keuzes gemaakt. De informatiebasis voor wat betreft gebouwen in METSELWERK-D is smal (berekeningen aan slechts 2 referentie-gebouwen zijn beschikbaar). Het betreft met name:

- De keuze voor de mediane seismische capaciteit. Deze is gebaseerd op de resultaten van één gebouw, wat het gebouw is met het hoogste berekende risico, wat vooral is bepaald door de grotere gevolgen bij bezwijken. Het is zonder uitvoerig nader onderzoek onduidelijk hoe deze uitkomsten veranderen als meer referentiegebouwen worden toegevoegd.
- De keuze voor toepassing van de mediaanshift is gebaseerd op andere typologieën bij gebrek aan informatie hierover voor METSELWERK-D.
- De keuze voor de gebouw-tot-gebouw spreiding $\sigma_{BB}$=0,30 is gekozen naar analogie van de bevindingen voor typologieën METSELWERK 1 en 2.

Om te onderzoeken of de gemaakte keuzes voldoende representatief zijn voor gebouwen van METSELWERK-D, is in Bijlage A een vergelijkende studie gepresenteerd waarbij gebruik is gemaakt van beschikbare berekeningen die door

NCG beschikbaar zijn gesteld en een beschikbare studie van een afstudeerder aan de TU Delft.
Vergeleken zijn de zogeheten backbone curves van de twee voor de afleiding van de typologie gebruikte referentiegebouwen met die van de extra gebouwen zoals deze doorgerekend zijn door ingenieursbureaus op basis van de NPR9998 (zie Tabel 5). Er blijkt een goede mate van overeenkomst te zijn tussen de resultaten, hetgeen vertrouwen geeft in het gebruik van de backbone curves in Figuur 3 voor de beschrijving van METSELWERK-D.

Ook zijn in bijlage A de NPR berekeningen van de seismische weerstand vergeleken met de belasting volgend uit de NEN Webtool, periode t5, dit kan worden beschouwd als een ‘bottom up’ benadering. Hieruit blijkt dat alle extra geanalyseerde gebouwen in ruime mate voldoen aan de NPR in alle gridpunten van de NEN webtool, ofwel overal in de provincie Groningen.

In hoofdstuk 7 wordt het risico voor METSELWERK-D berekend aan de hand van de parameters van paragraaf 4.3 tot en met 4.6. Dit is weergegeven in een kaart waarin het gebied waar het risico hoger is dan de Meijdam norm, is ingekleurd. Omdat uit de bottom up aanpak geen gebied wordt gevonden waar de geanalyseerde gebouwen niet voldoen aan de NPR 9998, geeft dit vertrouwen dat de keuze van de parameters voor METSELWERK D in de paragrafen 4.2 tot en met 4.6 tot voldoende veilige resultaten leidt.

Er wordt daarom geen aanpassing verricht aan de voorgestelde parameters in de tabellen 5 tot en met 7 voor de beschrijving van METSELWERK-D.

# 5 Sterkteparameters in de TNO modelketen-berekening voor METSELWERK-D

In dit hoofdstuk wordt op basis van de overwegingen gemaakt in hoofdstuk 4, inclusief de vergelijking met berekeningen uitgevoerd aan de hand van NPR 9998, het overzicht gegeven van de voor METSELWERK-D in rekening te brengen parameters voor het kwetsbaarheids- en gevolgmodel in de berekening met de TNO modelketen.

Tabel 9 toont de parameters voor het kwetsbaarheidsmodel en gevolgmodel zoals gebruikt voor het genereren van de vlekkenkaarten voor METSELWERK-D. Hoe deze parameters toegepast worden is beschreven in het hoofdrapport [TNO, 2021a].

Tabel 9: Overzicht van invoerparameters in de TNO modelketenberekening

| **Parameters** | **METSELWERK-D** |
|---|---|
| $b_{0lower}$ | -2,5932 |
| $b_{0middle}$ | -1,9877 |
| $b_{0upper}$ | -1,3822 |
| $b_0$ | -1,9877 |
| $b_1$ | 2,2622 |
| $\sigma_s$ | 1,0038 |
| DL_CS1 | 0,023 |
| DL_CS2 | 0,102 |
| DL_CS3 | 0,131 |
| Modelonzekerheid $\beta_m$ | 0,35 |
| Pd_inside\|CS1 | 0,0252 |
| Pd_inside\|CS2 | 0,0395 |
| Pd_inside\|CS3 | 0,42 |
| Pd_outside\|CS1 | 0,0402 |
| Pd_outside\|CS2 | 0,063 |
| Pd_outside\|CS3 | 0,67 |

# 6 Controles

De resultaten van de door TNO en TU Delft uitgevoerde analyses van beschikbare en aanvullende berekeningen leveren het sterktemodel op dat in de vorm van kwetsbaarheidskrommen in de TNO modellenketen is geïmplementeerd.

ACVG heeft in haar advies van november 2020 gevraagd een aantal controles uit te voeren [ACVG, 2020]. Dit betreft de volgende punten:

- Toon aan dat de aannames en interpretaties bij NLTH-berekeningen voldoende onderbouwd zijn.
- Toon aan dat de modellering van de gebouw-tot-gebouwvariabiliteit past bij de Groningse realiteit.
- Toon aan dat een uitgebreidere opname geen wezenlijke invloed heeft op het beoordelingsresultaat.
- Toon aan dat uit-het-vlak bezwijken correct is meegenomen in versimpelde (SDOF) modellen.

Voor een nadere toelichting op deze vier punten wordt naar het ACVG advies van november 2020 verwezen. Hieronder wordt kort beschreven welke controles voor METSELWERK-D zijn uitgevoerd. De twee eerste punten komen hieronder aan de orde. Het derde en vierde punt zijn reeds aan de orde geweest in het hoofdrapport [TNO, 2021a] en de rapporten voor METSELWERK 1 en 2 [o.a. TNO, 2021c]. Met betrekking tot het vierde punt wordt opgemerkt dat in bijlage A is aangetoond dat uit-het-vlak falen minder relevant is voor METSELWERK-D.

Als extra controle wordt verwezen naar de analyse in Bijlage A waarin push-over curves berekend door ingenieursbureaus direct zijn geïmplementeerd in een ADRS analyse conform NPR 9998.  Het blijkt dat alle geanalyseerde gebouwen voldoen aan de eisen uit NPR 9998.

## 6.1 NLTH berekeningen

Met betrekking tot de NLTH berekeningen is langs twee wegen invulling gegeven aan de gevraagde onderbouwing.

Als eerste is in Bijlage B.2 van het hoofdrapport [TNO, 2021a] een uitgebreide beschrijving gegeven van de aannames en interpretaties bij de NLTH berekeningen. Daarbij zijn deze tevens vergeleken en afgestemd met de aanpak zoals deze gevolgd is binnen NEN NPR 9998 module 3 [NEN, 2020].

Als tweede zijn de resultaten van de typologie -aanpak vergeleken met de uitkomsten van NLTH berekeningen en NLPO berekeningen uitgevoerd conform NPR 9998. Bijlage A van onderhavig rapport toont aan dat de NLTH berekeningen binnen de typologie-aanpak goed aansluiten bij deze extra informatie.

### 6.2 Gebouw tot gebouw variabiliteit

Voor de keuzes met betrekking tot mediaan en spreiding in de kwetsbaarheids-kromme wordt gerefereerd aan hoofdstuk 4. Op basis van de beschikbare informatie acht TNO het aannemelijk dat de resulterende kwetsbaarheidskromme een adequate beschrijving is van de seismische capaciteit van de Groningse gebouwenvoorraad binnen de typologie METSELWERK-D.

### 6.3 Vergelijking met NPR berekeningen

In bijlage A worden diverse beschikbare NPR berekeningen beschreven. In paragraaf 4.7 is geconcludeerd dat de typologie-aanpak conservatiever is dan elk van deze berekeningen. Dit geeft het vertrouwen dat de typologie-aanpak conservatief genoeg is.

# 7 Vlekkenkaart voor METSELWERK-D

Met de in Tabel 9 gegeven waarden voor de parameters voor de kwetsbaarheids- en sterktemodellen is met de TNO modelketen, op basis van de in [TNO, 2021a] gegeven instellingen, de vlekkenkaart voor METSELWERK-D bepaald.

De resulterende kaart is in Figuur 4 weergegeven. Voor meer achtergrond bij de totstandkoming van de vlekkenkaarten wordt verwezen naar het hoofdrapport [TNO, 2021a].

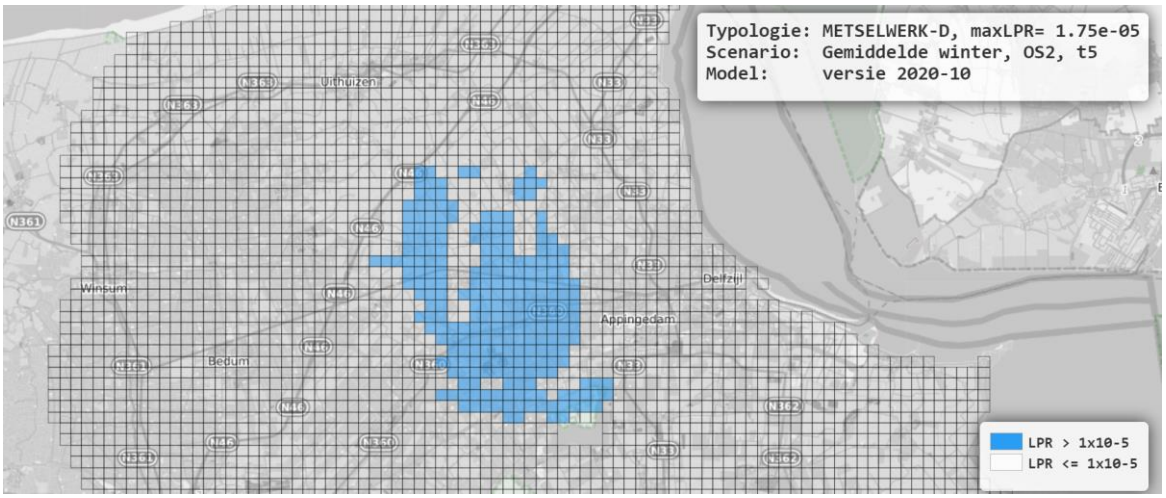


Figuur 4: Vlekkenkaart voor METSELWERK-D

Met blauw zijn de gridcellen ingekleurd waar gebouwen van METSELWERK-D niet voldoen aan de Meijdam norm [Meijdam, 2015]. Van die gebouwen moet worden vastgesteld of en in welke mate deze versterkt moeten worden.

# 8 Referenties

[ACVG, 2020]
Advies Typologieaanpak, 17 november 2020, ACVG kenmerk 202011-01

[Arup, 2016a]
LS-DYNA validation booklet, juli 2016

[Arup 2016b]
Arup, “Exposure Database V3”.

[Arup 2016c]
Arup, “Geometric characteristic study of current building selection for numerical modelling”, April 2016

[ARUP 2017a]
ARUP. Typology modelling: Analysis results in support of fragility functions - 2017 batch results. November 2017.

[Arup, 2017b]
Arup, Exposure database V5

[Arup 2017c]
Arup , Arup Project Title: Groningen Earthquakes - Structural Upgrading; Abel Eppensstraat – Development Phase Report, December 2017

[Arup 2017d]
Arup, Arup Project Title: Groningen Earthquakes - Structural Upgrading. Georg van Saksenlaan – Development Phase Report, December 2017

[Arup 2017e]
Arup Project Title: Groningen Earthquakes - Structural Upgrading De Rank 7-11b te Appingedam - Development Phase Report, December 2017

[Arup, 2019a]
Typology Modelling: Analysis Results in Support of Fragility Functions 2018–2019 Batch Results

[Arup, 2019b]
Typology Modelling - Typology Modelling Explicit MDOF Validation of Fragility Functions - URM3L - URM4L, 2019

[Arup, 2019c]
Typology Modelling: Analysis Results in Support of Fragility Functions – 2019 Batch Results, December 2019

[Arup 2019d]
Arup, “Exposure Database V7: Data Documentation, Technical Report and Exposure Model”, December 2019.

[Arup, 2020a]
LS Dyna Masonry Model recalibration, 4 mei 2020

[Brzev et al, 2013]
Brzev S., C. Scawthorn, A.W. Charleson, L. Allen, M. Greene, K. Jaiswal, V. Silva, 2013; GEM Building Taxonomy, version 2, GEM Foundation

[Crowley et al, 2015]
Helen Crowley, Rui Pinho, Barbara Polidoro and Peter Stafford, Report on the v2 Fragility and Consequence model for the Groningen Field

[Crowley et al, 2017]
Helen Crowley, Rui Pinho, Report on the v5 Fragility and Consequence Models for the Groningen Field, November 2017

[Crowley et al, 2019]
Helen Crowley, Rui Pinho and Francesco Cavalieri, Report on the v6 Fragility and Consequence Models for the Groningen Field, March 2019.

[Crowley et al, 2020]
Helen Crowley and Rui Pinho. Report on the v7 Fragility and Consequence Models for the Groningen Field. March, 2020.

[Esposito et al. 2018]
Esposito, R., Jafari, S., Ravenshorst, G.J.P., Schipper, H.R., and Rots, J.G. (2018) Influence of the behaviour of calcium silicate brick and element masonry on the lateral capacity of structures. In Proceedings of 10th Australasian Masonry Conference (AMC), 11-14 February, Sydney, Australia

[FEMA, 2012]
FEMA 58-1, Seismic Performance Assessment of Buildings, Volume 1, Methodology, FEMA, Washington DC, USA

[Meijdam, 2015]
Eindadvies Handelingsperspectief voor Groningen, Commissie Meijdam, December 2015

[NEN, 2020]
NEN Module 3 end conclusions. Concept version v02, Arup, BORG, TU Delft (8 - 12-2020).

[Noortman, 2019]
F. J. Noortman. Applicability of the pushover method for the seismic assessment of URM structures in Groningen: a case study of a low-rise apartment building, MSc thesis. February 2019.

[NPR, 2020]
NPR, Nederlandse Praktijk Richtlijn 9998, versie 2020

[TNO, 2021a]
Typologie-gebaseerde beoordeling van de veiligheid bij aardbevingen in Groningen - Achtergrond bij de methode, TNO Rapport 2020 R10628A, 2021

[TNO, 2021b]
Typologie-gebaseerde beoordeling van de veiligheid bij aardbevingen in Groningen – Typologisch toedelen, TNO Rapport 2021 R11002, TNO, 2021

[TNO, 2021c]
Typologie-gebaseerde beoordeling van de veiligheid bij aardbevingen in Groningen – Uitwerking van typologie METSELWERK1, TNO Rapport 2021 R10699A: TNO, 2021

[VIIA, 2019a]
VIIA, Technical Retrofit Advice of Rijksweg 107-117, December 2019.

[VIIA, 2019b]
VIIA, Technical Retrofit Advice of Rijksweg 119-129, December 2019.

[VIIA, 2020]
VIIA, Technical Retrofit Advice of Jachtlaan 16-18B and De Helling 2-6, April 2020.

# 9 Ondertekening

Delft, januari 2022 TNO

Ir.Ing. M. Steins-Zwanenburg

Dr. P.C. Rasker
Research manager
Structural Reliability

# A Vergelijking met beschikbare NPR berekeningen

## A.1 Introduction

To increase the confidence in the fragility and consequence model proposed for METSELWERK-D, TNO and TU Delft investigated the availability of studies on buildings that could be assigned to METSELWERK-D. For this purpose, TNO has received from the Nationaal Coördinator Groningen (NCG) assessments of buildings which are likely to be assigned to METSELWERK-D). The material received consisted of Technical Strengthening Advices (Technisch Versterkings Advies, TVA).
The material, obtained in different batches, was first reviewed to select those buildings which comply with the description of METSELWERK-D: regular floor plan (rectangular), number of storeys between three and five, concrete floors and unreinforced masonry (URM) walls. The other buildings in these batches were labelled as not conforming to METSELWERK-D. It was not further investigated for the purpose of this study whether and if so, to which extent, these could be assigned to a typology.
Only buildings assessed using non-linear push-over (NLPO),non-linear time-history (NLTHA) and non-linear kinematic (NLKA) analyses have been selected. From such analyses, capacity curves in terms of base shear and attic displacement capacity can be derived and compared to the ones of the index buildings selected for METSELWERK-D (Figure A.1). The overview of the material received is given in Appendix C. From the 28 TVAs available, 6 are selected for the analysis. In one TVA (De Helling 6-8 and Jachtlaan 16-18B) the building is divided in 2 partitions which are analysed separately (see Table A.1). On the other hand, 2 TVAs (Rijksweg 107-117 and Rijksweg 119-129) considered similar buildings and their assessment was identical. Due to this, the number of available analyses (buildings) is still 6.

Figure A.1 Side view of Koeriersterweg (left) and Schuitenzandflat (right), index buildings of METSELWERK-D (source: Google Street View).

In addition to the selected TVAs, this appendix describes the findings of the TU Delft Master thesis [Noortman, 2019], carried out in collaboration with Royal Haskoning DHV (RHDHV).

[Noortman, 2019] studied the seismic behaviour of a 4 storey apartment building with an unreinforced masonry load-resisting system. This building was investigated

in terms of non-linear pushover analyses (NLPO), non-linear time-history analyses (NLTH), modal response analyses (MRS) and a Macro Equivalent Frame analyses (MEF). In this appendix, the results of the NLTH and NLPO analyses reported in [Noortman, 2019] are compared to the index buildings adopted for METSELWERK-D (respectively, Koeriersterweg and Schuitenzandflat). The buildings are compared in terms of backbone curves and collapse mechanisms observed in the NLPOs and NLTHAs analyses.

Section A.2 describes the methodology applied for the analyses. Section A.3 to A.6 outline the analyses of the selected buildings. The information used is summarized in Table A.1. Section A.7 provides conclusions based on the analyses in this annex.

Table A.1 Summary of the analyses adopted in this study.

| Identifier | Source | Address | Analysis type | Par. |
|---|---|---|---|---|
| [Noortman, 2019] | TuD | Not mentioned in the report | NLTHA[1], NLPO | A.3 |
| DELF_RIJKSW_AG | NCG | Rijksweg 107-117 and Rijksweg 119-129 | NLPO, NLKA | A.4 |
| DELF_DEHELL_AG | NCG | De Helling 6-8 and Jachtlaan 16-18B | NLPO, NLKA | A.5 |
| APPD_DERANK_AG | NCG | De Rank 7-11B | NLTHA[2] | A.6 |
| APPD_AEPPEN_GF | NCG | Abel Eppensstraat 15-69 | NLTHA[2] | A.6 |
| APPD_GVSAKS_AG | NCG | Georg van Saksenlaan 27-37B | NLTHA[2] | A.6 |

[1] Analysis performed using incremental time series.

[2] Analysis according to NPR 9998: 2015.

## A.2 Methodology

The results of available analyses performed on buildings which can be assigned to METSELWERK-D are discussed in this section based on the following steps.

Table A.1 summarizes the analyses that were used for this study. There are 3 types of analyses, NLPO, NLKA and NLTHA respectively:

- NLPO derives push-over curves that describe the in-plane seismic capacity. From these curves, bilinear curves are derived according to NPR 9998:2020 and are compared to the t5 response spectra of the NEN webtool. The procedure is described in section A.2.1.
- NLKA checks out-of-plane failures and the procedure is described in A.2.2.
- Two types of NLTHA simulations are available: incremental and NPR 9998: 2015 based. From the incremental NLTHA, a backbone curve is derived and compared to the NLPO push-over curves and compared to the webtool. The NLTHA based on NPR 9998: 2015 cannot be used to derive backbone curves but are used to investigate the collapse mechanisms. The description of the procedure for NLHTA is discussed in A.2.3.

### *A.2.1 NLPO analyses*

First, the seismic capacity and collapse mechanisms observed for the available buildings are compared to those of the index buildings adopted for METSELWERK-D. To compare the seismic capacity, capacity curves are derived from non-linear push-over (NLPO) analyses. The capacity curves are reported in terms of normalized forces, which are obtained by normalizing the shear force at the base of the buildings by the dynamic weight of the building, which represents the (inertial) force acting on the building.
From the capacity curves, the performance of the building with respect to in-plane collapse is assessed according to the recommendations provided in NPR 9998:2020. In particular, TNO and TU Delft evaluated the performance related to in-plane global collapse mechanisms of the analyzed material according to the appendix G of NPR 9998:2020. For this purpose, bilinear curves are derived from the capacity curves and the compliance of the building is checked using the Acceleration-Displacement Response Spectra (ADRS) computed from the NEN webtool, version v6, period t5. In detail, the spectra adopted from the NEN webservice are selected using the inputs provided in Table A.2. This is the same hazard as adopted for the risk evaluation of the METSELWERK-D typology. The compliance is checked for every cell in the NEN grid (see Figure A.2), to which a different color can be assigned when the capacity doesn't satisfy the seismic demand.

Table A.2 Parameters adopted for the evaluation of the elastic spectra from the NEN webservice.

| Parameter | Value |
|---|---|
| Version | V6 |
| Position | Surface |
| Period | t5 |
| Return time | 2475 years |

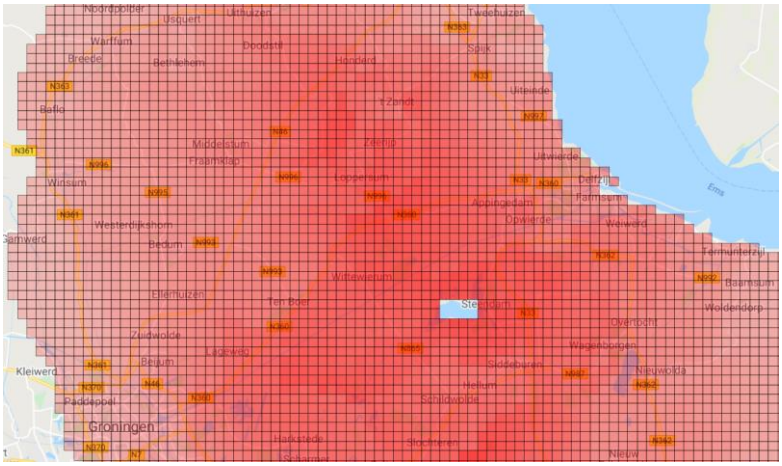


Figure A.2 Grid cells provided by the NEN webservice for which response spectra are available.

To compare the capacity curves and ADRS curves according to the procedure described in Appendix G of NPR 9998: 2020, bilinear curves are considered. Those

are characterized by the yield and ultimate (near-collapse) displacements ($d_y$ and $d_u$) and accelerations ($a_y$ and $a_u$), and the total damping ($\xi_{sys}$). The parameters are obtained from the engineering reports when available. Otherwise, they are computed starting from the normalized capacity curves following Appendix G of NPR 9998: 2020. To construct ADRS curves, response spectra are first derived from the NEN website (https://seismischekrachten.nen.nl/map.php), with the setting described in Table A.2. From the NEN website, the following parameters can be obtained from each cell $T_B, T_C, T_D, a_g$ and $p$ where: $T_B$ and $T_C$ are, respectively, the starting and ending periods of the constant spectral acceleration part (plateau) of the spectra, $T_D$ is the starting period of the constant spectral displacement part of the spectra, $a_g$ is the peak acceleration at ground level and $p$ is the ratio between the spectral acceleration at the plateau and ground level (amplification factor).

From these parameters, the elastic spectra can be computed following the NPR 9998:

$$S_e(T) = \begin{cases} a_g \left[1 + \frac{T}{T_B}(\eta \cdot p - 1)\right] & T \le T_B \\ a_g \cdot \eta \cdot p & T_B < T \le T_C \\ a_g \cdot \eta \cdot p \cdot \frac{T_c}{T} & T_C < T \le T_D \\ a_g \cdot \eta \cdot p \cdot \frac{T_c \cdot T_D}{T^2} & T > T_D \end{cases}$$

Where $\eta$, the dimensionless damping correction factor is assumed 1 for damping $\xi_{sys} = 5\%$. From the elastic spectral accelerations, $S_e(T)$ the elastic spectral displacement $S_{De}(T)$ are computed as:

$$S_{De}(T) = S_e(T) \cdot \left(\frac{T}{2\pi}\right)^2$$

The ADRS spectra is the curve obtained by plotting $S_{De}$ against $S_e$. To account for energy dissipation and damping in the structure, the ADRS spectra is scaled by the spectral reduction factor, $\eta_\xi$:

$$\eta_\xi = \sqrt{\frac{7}{2 + \xi_{sys}}} \le 0.55$$

Where $\xi_{sys}$ is the total damping of the system, which is obtained as the sum of the inherent damping, $\xi_0$, and the hysteretic damping:

$$\xi_{sys} = \xi_0 + \xi_{hys} + \beta_0$$

Where for unreinforced masonry, $\xi_0$ is 5% as prescribed by NPR 9998: 2020. As conservative assumption, the contribution of the foundation $\beta_0$ to the total damping is neglected. The hysteretic damping is obtained by Table G.3 of NPR 9998: 2020:

$$\xi_{hys} = 0.42\left(1 - \frac{0.9}{\sqrt{\mu_{sys}}} - 0.1\sqrt{\mu_{sys}}\right) \le 0.15$$

In which $\mu_{sys}$ is the system ductility, computed as follows:

$$\mu_{sys} = \frac{d_u}{d_y}$$

$d_u$ and $d_y$ are, respectively, the NC and the yielding displacement of the equivalent SDOF bilinear capacity curve. Using these values, the spectral reduction factor $\eta_\xi$ is computed and compliance is checked. It is noted that although damping depends on mobilized ductility, it can be shown that if only a compliance check is required, compliance is ultimately governed by the damping at NC if the capacity not already satisfies the demand of the original ADRS curve at 5% damping. Iteration is not needed for a compliance check.

### *A.2.2 NLKA*

The safety related to out-of-plane mechanisms using NLKA is not directly assessed by TNO, but it refers to the outcomes of the assessments reported in the available analysis reports.
When the global assessment of the building is based on NLPO analyses, the local assessment of the out-of-plain collapse is performed via non-linear kinematic analyses (NLKA).
All the NLKA described in the studies summarized in table A.1 are performed by the consultants in accordance with the recommendations reported in the Annex H of NPR 9998:2018. This is a displacement based inelastic method which requires to compute separately both the capacity and the seismic action acting on each wall.
The NLKA method is based on the principle of virtual work. For this reason, the failure mechanism of the wall should be assumed in advance. The version of Annex H in NPR9998:2018 provides solutions for one-way vertically spanning walls only.
Depending on the boundary conditions, four different configurations are possible:

- Vertical span, for masonry walls spanning between floors;
- Gable end, for gable walls with adequate restraint at roof level;
- Cantilever, for parapets, partition walls and gables not supported at roof level;.
- Chimneys, which is a modification of the cantilever solution.

The capacity of the walls is provided in a graphical form in Figures H.3 to H.7 of Annex H, as function of the geometry of the wall, of the boundary conditions and of the overburden load acting at the top of the wall.
The demand acceleration is computed starting from the base acceleration of the building, and takes into account the possible amplifications determined by the position of the wall at higher levels and by the interaction between the vibration period of the wall and of the whole building. The formula provided in Annex H to compute the demand acceleration (H.3) is adapted from NEN-EN 1998-1 to compensate for potential unconservative de-amplification for very short periods.

### *A.2.3 NLTH analyses (NLTHA)*

As mentioned there are two types of NLTHA available, see table A.1. Each type is investigated differently.

*Incremental NLTHA:*
For the incremental NLTHA, the maximum base shear and displacements of each record are computed to determine a capacity curve. The curves are reported in terms of normalized forces, which are obtained by normalizing the shear force at the base of the buildings by the dynamic weight of the building, which represents the (inertial) force acting on the building. These capacity curves can be directly compared to the backbone curves of the index buildings adopted for

METSELWERK-D. For the incremental NLTHA in table A.1 also a NLPO is available. The two capacity curves will be compared and will be used to check for compliance in all the NEN grid cells using the webtool, version v6, period t5. This is the same hazard as adopted for the risk evaluation of METSELWERK-D. Besides this compliance check, collapse mechanisms are also reviewed.

*NLTHA according to NPR 9998: 2015:*
When NLTHA are performed to assess the global performance of the building, those are able to describe also the local out-plane collapse of walls, either via the explicit simulation of the wall collapse or indirectly via the check of the wall out-of-plane deflection. The NLTHA based on NPR 9998: 2015 cannot be used to derive backbone curves, nor can the results be used to check compliance of a building against the webtool, version v6, period t5, the hazard used in the risk evaluation of METSELWERK-D. These NLTHA analyses are used to investigate the collapse mechanisms both in-plane and out-of-plane as far as it is possible to deduct from the available studies.

## A.3 Noortman, 2019

### *A.3.1 Description*

The building investigated by [Noortman, 2019] can be described as a medium-rise URM apartment building made of 4 stories with concrete floors and roof. Due to privacy reasons, the exact location of the building within the Groningen area is not known, thus the building will be hence referred to as [Noortman, 2019]. Figure A.3 shows a picture of the building, which is made of repeated modules with the same wall configurations. Due to this, only a module (unit) of the building was analysed in [Noortman, 2019] to reduce the computation time and computational demand.

Figure A.3 Picture of the low-rise URM apartment building analysed in [Noortman ,2019]. Source: [Noortman, 2019].

Figure A.4 shows the layout of the building, which highlights the almost complete absence of load-bearing walls in the longitudinal (weak direction) compared to the transverse direction (strong direction). In particular 2 load-bearing walls, 2.4 m long and 200 mm thick, are the only load-resisting elements in the weak direction, as a result of a wind-resistant design.

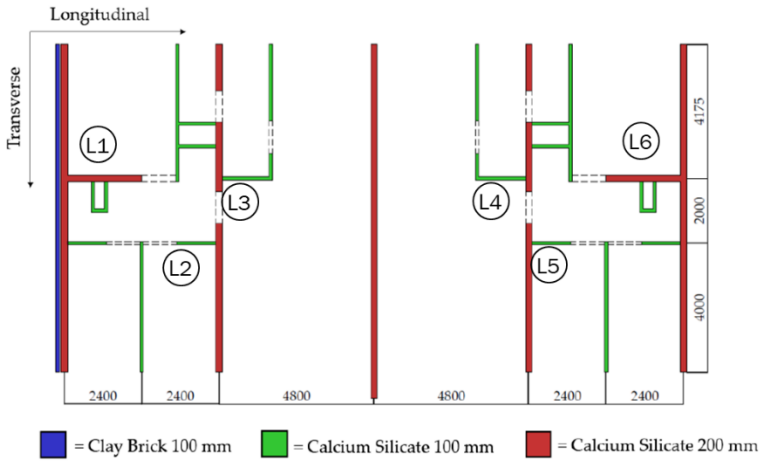


Figure A.4 Wall configuration of the first floor of the low-rise URM apartment building adopted in [Noortman, 2019]. In the figure, the longitudinal wall for which the cracks are observed are indicated with the L; Source [Noortman, 2019].

Figure A.5 shows a side view of Koeriersterweg and Schuitenzandflat index buildings adopted respectively for MW-D typology.

Figure A.5 Side view of Koeriersterweg (left) and Schuitenzandflat (right), index buildings of METSWELWERK-D(source: Google Street View).

The material and geometric properties of the building investigated in [Noortman, 2019] match best the description of Schuitenzandflat and, for this reason, the results [Noortman, 2019] will be compared to Schuitenzandflat index building. The results of the NLTHA on Schuitenzandflat can be found in [ARUP (2017a,2019a,2020a)]. It should be noted that, differently from Noortman, 2019, the resistance to horizontal load in the weak direction is mainly provided by the URM piers of the façades of this index building.

### *A.3.2 Backbone from NLPO and NLTHA analyses*

Both NLPOs and NLTHAs were performed in the study of [Noortman, 2019]. Figure A.6 summarizes the results of the NLPO analyses in terms of base shear and displacement of the control node (selected at the attic level) in both transverse (strong) and longitudinal (weak) directions, using modal and uniform load distributions and using either DIANA (FEM) or 3MURI (EFM) to perform the analyses. Among all the curves presented, the longitudinal direction is the

governing direction. From the study, it was also concluded that 3MURI typically tends to underestimate the capacity of the building. For this reason, the push-over curve obtained using DIANA is adopted for the comparison with the Schuitenzandflat index building. The modal load distribution is selected for the comparison because it is the one that returns the lowest estimated capacity for the building.

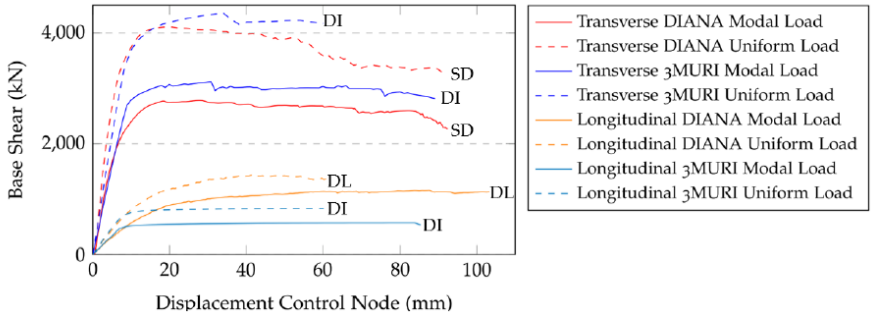


Figure A.6 Capacity curves obtained in [Noortman, 2019] in longitudinal and transverse direction using different load distribution (modal/uniform) and different software (DIANA/3MURI). The analyses are stopped when either strength degradation (SD), exceedance of drift level (DL) limits or dynamic instability (DI) is observed.

Note that the push-over curves are stopped because the drift limits defined in NPR 9998 for near collapse are exceeded. This implies that the real collapse displacement is larger than the current push-over curve (although it is not possible to quantify how much larger). Other than the NLPO simulations, 7 NLTHA analyses are provided for different signals, shown in Figure A.7. From these NLTHA, an average curve was estimated.

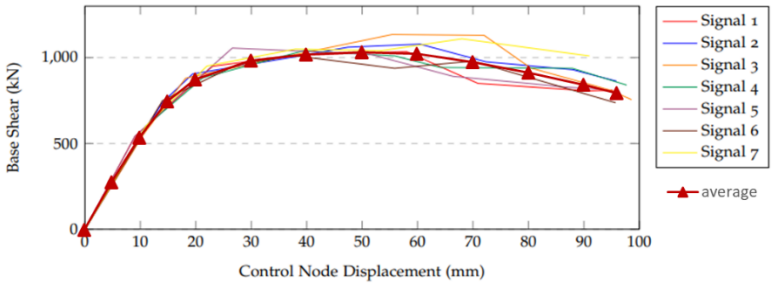


Figure A.7 Capacity curves obtained from the NLTHA in [Noortman, 2019] in longitudinal (weak) direction. From the many capacity curves, an average curve (indicated with triangles and a red solid line) is estimated.

The associated effective mass related to the DIANA model in the longitudinal direction is 5003kN. This mass is used to normalize the curves defined for both the push-over and NLTH analyses and compare them to the backbone curve of Schuitenzandflat from [Crowley et al 2020]. Figure A.8 shows the comparison between the normalized capacity curves from [Noortman, 2019] and the backbone curve of MW9 index building (Schuitenzandflat). From the figure, the following can be observed that a good agreement exists in terms of normalized base shear between the 3 curves. However, both the NLPO- and NLTH-based backbone curves present a smaller displacement compared to index building. This can be

explained form the fact that the NLPO and NLTH analyses are not pushed up to collapse (or divergence of the analyses) and are instead stopped when strength degradation (drop in base shear of 20% relative to the peak value) or the drift limits defined in NPR 9998 are exceeded. Due to this and to the steep of the softening branch of the NLTH backbone curve up to the point where the analyses were stopped, it is expected that the backbone curve would have a similar collapse displacement of the index building.

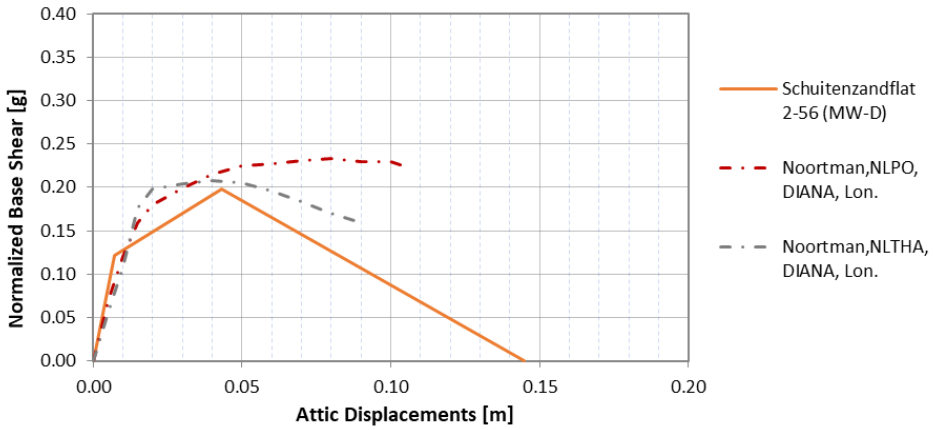


Figure A.8 Comparison between the backbone curves obtained from the NLTHAs and NPLO in [Noortman, 2019] and the one of Schuitenzandflat, index building of METSELWERK-D (MW-D).

### *A.3.3 Collapse mechanisms*

The collapse mechanisms observed in [Noortman, 2019] reported an exceedance of the drift limits at the storey between ground and first-floor level, which implies an in-plane failure of the load-bearing walls in the longitudinal direction. Figure A.9 shows the drift limits observed in each of the NLTHA performed in the study and the crack pattern observed in one of the NLTHA on the longitudinal walls. Out of those 6 walls shown in the figure, only L1 and L6 are load-bearing walls (i.e. connected at floor level). From the drift limits and the crack pattern, it can be seen that the failure is localised at the storey between ground and first floor levels characterised by a shear diagonal failure of the load-bearing piers, subsequent to large rocking deflections. For this reason, the drift limits related to ductile failure mechanisms were selected. This is also concluded in the study, supported by the observation of the bed joint and head joint parameters. The collapse is expected to be similar to that observed in the experimental tests performed in 2016 at TU Delft (see [Esposito et al. 2018]) on a full-scale masonry assemblage representing the load-bearing structure of a terraced house (Figure A.10).

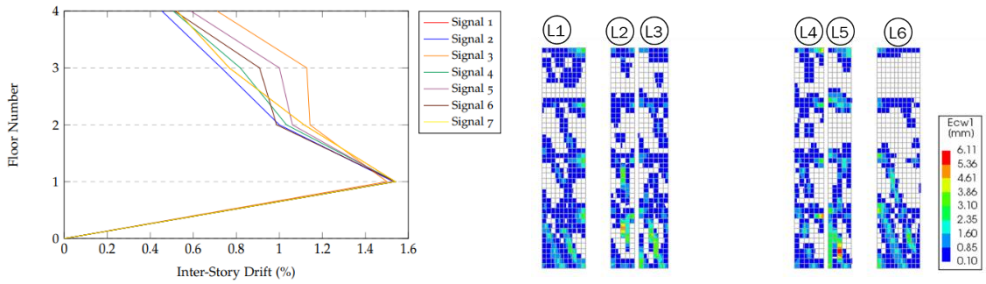


Figure A.9 Inter-story drift observed in each NLTHA (left) and crack patterns observed in the longitudinal walls. Out of those, only L1 and L6 are load-bearing walls. Source: [Noortman, 2019].

Figure A.10 Damage at the end of the test performed at TU Delft on a full-scale assemblage representing the load-bearing structure of a terraced house. From [Esposito et al. 2018].

The failure mechanisms observed in Schuitenzandflat index building, reported in [Arup, 2017,2019a,2020a], was also localised at the storey between the ground and first-floor level. The failure is related to toe-crushing of the piers at the first-floor level (up to the third floor, Figure A.11). Although this failure mode looks different from the one shown in [Noortman, 2019], the two failure modes are both characterized by large initial displacements due to the horizontal cracks at the bottom and top of the piers which allow for a rocking mechanism. The eventual collapse is due to either shear diagonal failure or toe crushing and it is sudden in both cases, but the overall structural behaviour is rather ductile.
It should be noted that Arup has re-calibrated in 2020 the parameters in compression of the constitutive model used in LS-DYNA for masonry (Arup, 2020a). This new calibration was performed to better match the experimental results of an in-plane test which ended with the collapse of the specimen due to toe-crushing. Analyses of the Schuitenzandflat index building were performed with the model both before and after the re-calibration: the identified failure mechanism does not change, but the outcomes of the simulations with the re-calibrated model show an even more ductile behavior of the building. Since ARUP advises to consider the most recent simulations as a sensitivity study, the backbone curve defined with the original properties for the constitutive model is used, which can be considered a conservative solution (being characterized by lower ductility).

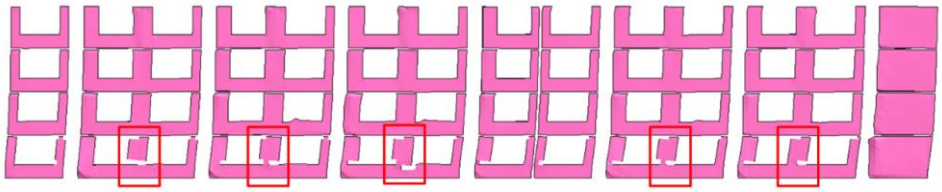

Figure A.11 Toe-crushing collapse mechanism observed in the squat piers at first storey level (storey between first and second floor). The governing failing piers are highlighted by red rectangles where the elements failed due toe-crushing are deleted. From [ARUP (2020)]

### *A.3.4 Definition of the equivalent bilinear curves (according to NPR 9998 [NPR, 2020])*

To evaluate the safety of a building with respect to in-plane global collapse mechanisms according to appendix G of the NPR 9998: 2020, an equivalent bilinear-curve is estimated from the results of the pushover analyses. For the building analyzed in [Noortman, 2019], this is obtained from the push-over curve shown in Figure A.8 for which the initial (elastic) stiffness $k_{init}$, maximum displacement ($d_{max}$), peak base shear ($V_b$), effective mass ($m_e$) and participation factor are provided in Table A.3.

First, the push-over curve is scaled using the participation factor $\Gamma$, and then the total energy, $E_m$, corresponding to the area of the curve, is computed. Second, a SDOF push-over curve normalized with respect to the effective weight, $m_e g$, and the maximum normalized base shear of the bilinear curve, $a_u$, is obtained by imposing the equivalence of the energy:

$$a_u = \frac{d_{max}\, k_{init} - \sqrt{(d_{max}\, k_{init})^2 - 2E_m\, k_{init}}}{m_e g}$$

Table A.3 Parameters derived from [Noortman (2019] to define an equivalent bilinear curve.

| **Building** | **Ref.** | $\boldsymbol{k_{init}}$ $[\boldsymbol{kN/mm}]$ | $\boldsymbol{d_{max}}$ $[\boldsymbol{mm}]$ | $\boldsymbol{V_b}$ $[\boldsymbol{kN}]$ | $\boldsymbol{m_e}$ $[\boldsymbol{ton}]$ | $\boldsymbol{\Gamma}$ $[-]$ |
|---|---|---|---|---|---|---|
| Noortman, 2019 | [Noortman, 2019] | 66 | 103.4 | 1159 | 500.3 | 1.35 |

Figure A.12 shows the original push-over curve, the SDOF-transformed push-over curve and the equivalent bilinear curve. To ease the representation, the curves are already normalized with respect to the effective weight. Table A.3 provides the parameters that define the bilinear curve.

The parameters of the bilinear curve are used also to define the damping of the system, which is estimated according to the NPR 9998: 2020. The system ductility $\mu_{sys}$ is computed equal to 6.32. Since the hysteretic damping for a system ductility of 6.32 corresponds to 16.4%, the hysteretic damping of the system is taken as the upper bound of 15%.
Finally the total damping is obtained as the sum of the inherent damping, $\xi_0$ (equal to 5%), and the hysteretic damping, leading to a total damping of $\xi_{sys}$= 20%.

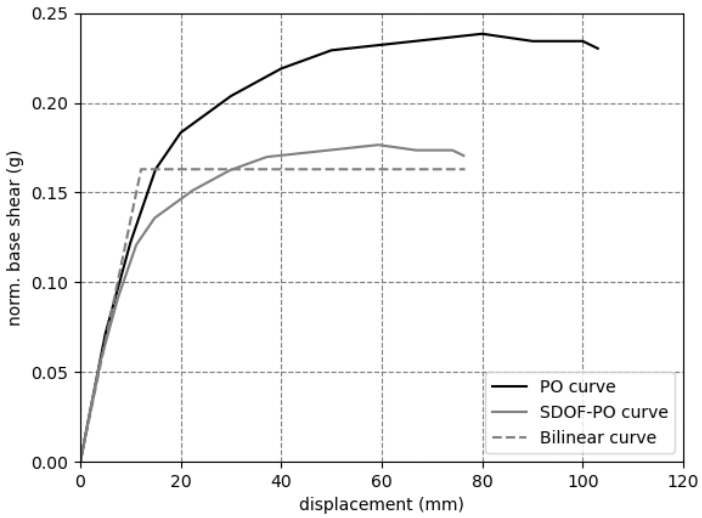


Figure A.12 Original push-over curve, the SDOF-transformed push-over curve and the equivalent bilinear curve computed from [Noortman, 2019] in terms of displacement and normalized base shear.

Table A.4 Yield and near-collapse points of the bilinear curves derived from [Noortman, 2019] and corresponding total damping.

| **Building** | **Ref.** | $d_y$ $[mm]$ | $d_u$ $[mm]$ | $a_u$ $[g]$ | $\xi_{sys}$ [%] |
|---|---|---|---|---|---|
| Noortman, 2019 | [Noortman, 2019] | 12.1 | 76.6 | 0.163 | 20.0 |

### *A.3.5 Safety assessment using NPR 9998*

The assessment described in this section is based on the global performance of the building using acceleration-displacement response spectra (ADRS) which are compared against the bilinear curve in Table A.3. The compliance of the bilinear curve is checked for cell of the NEN webtool and for each curve the performance indicator, i.e. the ratio between the building capacity and the seismic demand at the performance point. Figure A.13 shows the bilinear curve against all the elastic and inelastic (damped) ADRS while Figure A.14 presents the distribution of the performance indicators for the building investigated in [Noortman, 2019] over the NEN grid. The minimum performance indicator corresponds to 2.04 for this building. Since the bilinear curve is compliant to all the ADRS curves, none of the NEN cells are unsafe with respect to the global in-plane failure of the buildings and thus the corresponding cells in the map are empty. For this reason, the map is not presented in this section.

In addition to the global assessment of the building, the local failure mechanisms, and especially the out-of-plane failure of the walls, must also be assessed. Since the study in [Noortman, 2019] focuses on a comparison between the NLTHA and the NLPO methods, it does not include any explicit check of the out-of-plane performance of the walls, but the NLTHA provides an indirect check for it. The only failure mode reported regards the in-plane collapse of the piers at the storey between ground and first-floor level, as described in section A.3.3, but no collapse

of the walls in the out-of-plane direction is documented. For this reason, accounting for the local out-of-plane failure mechanism would not modify the outcomes of the vulnerability assessment as presented in this section.

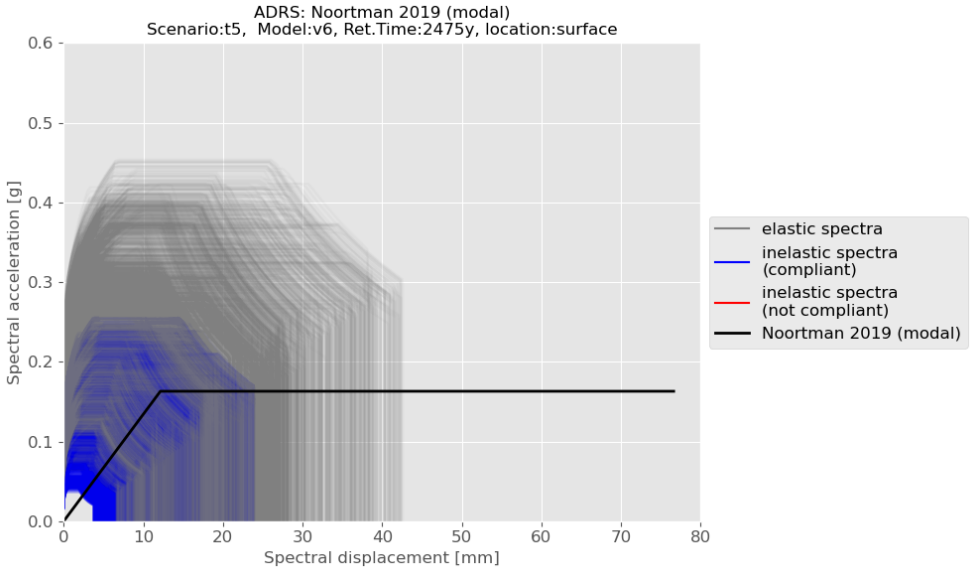


Figure A.13 ADRS spectra (elastic in grey and inelastic in blue) against the bilinear curves of Noortman, 2019 (solid black line); Bottom: corresponding distribution of the performance indicators.

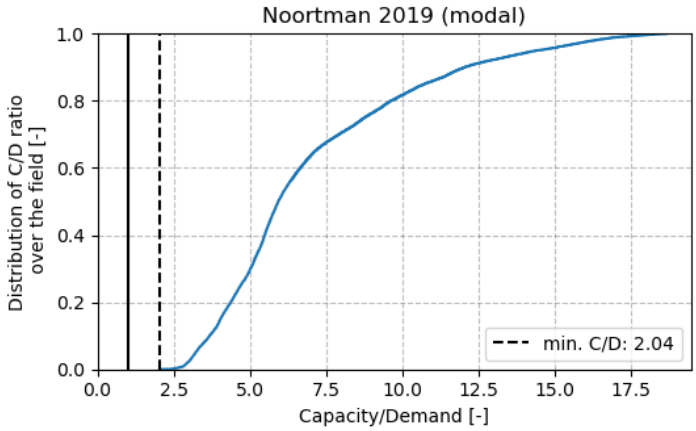


Figure A.14 Distribution of the performance indicators (ratio between capacity and demand) over the NEN grid for the bilinear curve of Noortman, 2019. The capacity over demand ratio of 1 is indicated with a black vertical solid line while the minimum ratio computed from the ADRS curves is indicated with a black vertical dashed black.

## A.4 Rijksweg 107-117 and Rijksweg 119-129

### *A.4.1 Description*

Rijksweg 107-117 and Rijksweg 119-129 are 4 storey terraced apartment buildings plus an attic (see Figure A.15 and Figure A.16). The buildings are characterised by URM cavity walls, concrete floors (except for a timber floor at the attic level) and a pitched roof. The configuration and geometry of the two buildings is the same, except that they are mirrored (compare Figure A.15 and Figure A.16). Due to a similarity with another building previously assessed by VIIA, Rijksweg 101-105, both Rijksweg 107-117 and Rijksweg 119-129 were assessed by VIIA using the outcome of the analyses performed on Rijksweg 101-105. Therefore, only the results for Rijksweg 107-117 are presented in this section given that the outcome is also applicable to Rijksweg 119-129. Figure A.17 shows the configuration of the walls at the first-floor level and the attic level. The buildings have a regular plan and a regular wall configuration across the height, except for the ground floor that has smaller openings compared to the upper floors. The buildings present load-bearing wall spanning along the longitudinal and transverse direction (respectively X and Y in Figure A.17). At the attic level, gable walls support the roof structure spanning along the transverse direction.

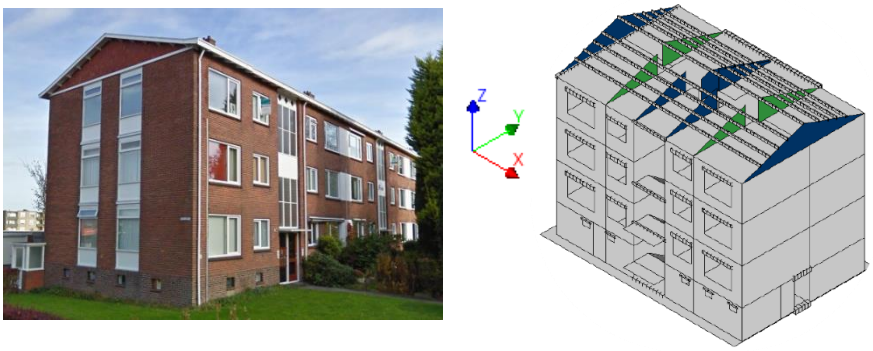


Figure A.15 Rijksweg 107-117, Delfzijl: side view (left, taken from Google Street View) and corresponding FEM model (right) adopted in [VIIA 2019a].

Figure A.16 Rijksweg 119-129, Delfzijl: side view (left, taken from Google Street View) and corresponding FEM model (right) adopted in [VIIA 2019b].

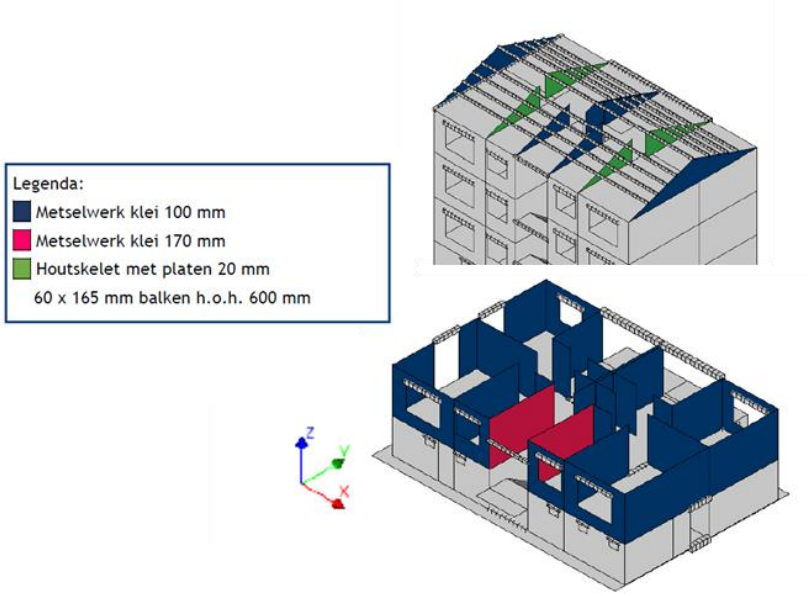


Figure A.17 Wall configuration at the attic level (top) and first floor (bottom) adopted for the FEM model of Rijksweg 107-117 in [VIIA 2019a] and Rijksweg 119-129 in [VIIA 2019b].

Other key assumptions for the analyses include: (i) the connections between all constructive elements (walls, floors, roofs) are assumed to be fixed. (ii) Small piers with a width of less than 500 mm are assumed to have bearing capacity only in the vertical direction. For Rijksweg 107-117, the NLPO analyses were carried on both longitudinal and transverse directions. The out-of-plane capacity of the walls is checked using a non-linear kinematic analysis (NLKA).

It should be noted that for Rijksweg 107-117 and Rijksweg 119-129, the analyses are stopped when the drift limits at near collapse, recommended in NPR 9998, are exceeded at one of the floor levels. Since progressive collapse is not modelled explicitly as in [ARUP 2019], the real collapse displacement of the buildings investigated in [VIIA 2019a, 2019b] is expected to be larger than the one reported in the capacity curves, although it is not possible to quantify how much larger. For both buildings, the FE package DIANA FEA was adopted to perform the NPLO analyses.

### *A.4.2 Backbone from NLPO analyses*

The NPLO analyses provided in [VIIA 2019a, 2019b] are compared against the capacity curves (the so-called backbone curves) of the index buildings of METSELWERK-D.

Figure A.18 shows the capacity curves of Rijksweg 107-117 and Rijksweg 119-129 in the transverse and longitudinal direction, since the presence of load-bearing walls in both directions makes it hard to identify a-priory the governing (weaker) direction. The post-peak behaviour of Rijksweg 107-117 and Rijksweg 119-129 was not investigated thus the real ductility of the building is unknown. Figure A.18 confirms that push-over curve adopted to analyze both buildings are coinciding and therefore only Rijksweg 107-117 is compared against the index buildings adopted for METSELWERK-D.

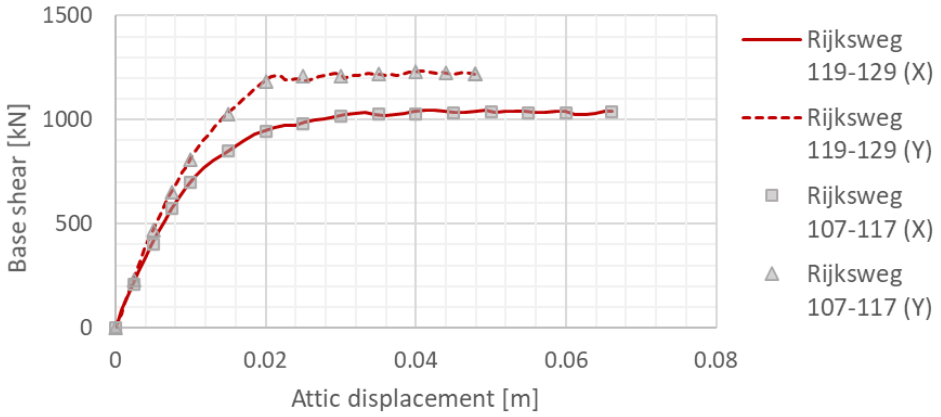


Figure A.18 Capacity curves extrapolated from [VIIA 2019a, 2019b] for Rijksweg 107-117 and Rijksweg 119-129 for X and Y direction.

To compare the curves of Rijksweg, Schuitenzandflat and Koeriersterweg to each other, first the base-shear capacity has to be normalized by the effective weight of the building, obtained by the product between the effective mass ($m_e$) and the gravity acceleration ($g$). However, since neither the effective mass nor the mode shape and mass distribution are provided in [VIIA 2019a, 2019b], the total dynamic weight is used instead (i.e. the transformation factor Γ is assumed to be equal to one). It should be noted that this is a conservative assumption since the larger the weight, the smaller is the normalized base shear (and the total dynamic weight is larger than the effective weight). For Rijksweg 107-117 this means that the normalized base-shear is expected to be larger, although the precise value cannot be quantified. The adopted values of the dynamic mass related to each capacity curve presented in Figure A.18 are listed in Table A.5.

Table A.5 Dynamic weight adopted from the analyses to normalize the base-shear capacity of the capacity curves.

| Curve | Dynamic weight [kN] |
|---|---|
| Rijksweg 107-117 (X) | 3785.71 |
| Rijksweg 107-117 (Y) | 3785.71 |

Figure A.19 shows the capacity curves in Figure A.18 after scaling by the dynamic weight together with the backbone curve of Koeriersterweg and Schuitenzandflat.

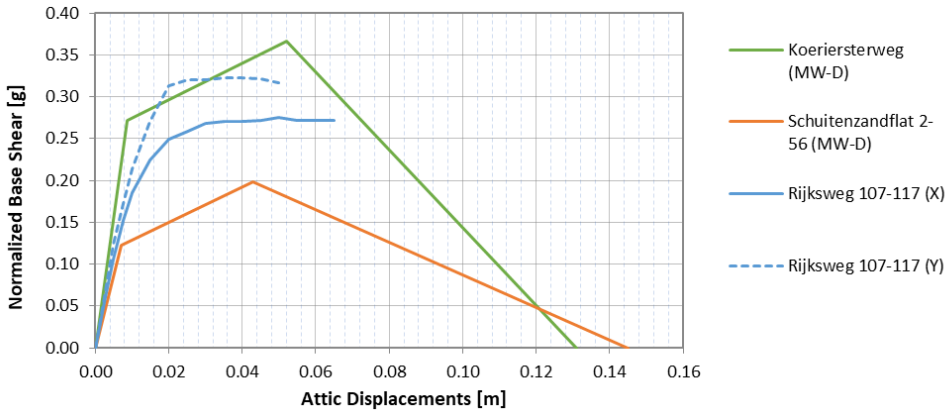


Figure A.19 Normalized capacity curves obtained from [VIIA 2019a] compared against the backbone curves selected for METSELWERK-D (MW-D).

From the figure, the following was observed: A good agreement is found between Koeriersterweg and Rijksweg 107-117 at least until the peak force is reached. However post-peak behaviour of Rijksweg 107-117 was not investigated since the curves are stopped when drift limits or the drift limits defined in NPR 9998 are exceeded. Progressive collapse is not explicitly modelled as for Koeriersterweg.

For this specific typology, the fragility of the buildings at collapse is mostly driven by the displacement capacity. Table A.6 provides the median of the full-collapse fragility functions of Koeriersterweg and Schuitenzandflat, together with the peak normalized base shear and collapse displacement of the backbone curves. From the table, it is observed that the median of the fragility function of Schuitenzandflat is slightly larger than Koeriersterweg even though the base shear capacity of Koeriersterweg is much larger. This can be explained by the larger collapse displacement of Schuitenzandflat.

Table A.6 Median of the fragility functions of Koeriersterweg and Schuitenzandflat at full collapse.

| Index building | Median [g] | Peak acceleration [g] | Collapse displacement [mm] |
|---|---|---|---|
| Koeriersterweg | 1.15 | 0.367 | 131 |
| Schuitenzandflat | 1.21 | 0.198 | 145 |

### *A.4.3 Collapse mechanisms*

The collapse mechanisms observed in [VIIA 2019a] only concerned in-plane collapse mechanisms since NLPOs are inherently unable to detect out-of-plane collapse mechanisms. Out-of-plane (OOP) mechanisms are checked for using NLKA methods. No full-collapse of Rijksweg 107-117 is reported in [VIIA 2019a], since the loadbearing structure does not show deficiencies for the seismic demand corresponding to the location of the building. Only the OOP capacity of the outer leaves is insufficient: this is expected to remain a local collapse but the progressive collapse is not modelled. Conversely, in Koeriersterweg the out-of-plane collapse of the gable walls at the attic level determines the collapse of the attic storey level and initiate the full collapse of the building. A detailed description of the collapse

mechanisms of Koeriersterweg can be found in [Arup, 2017, 2019a, 2020a]. The capacity curve can be used to compare between Koeriersterweg and Rijksweg 107-117. The same conclusions hold for Rijksweg 117-129.

### *A.4.4 Definition of the equivalent bilinear curves (according to NPR 9998 [NPR, 2020])*

For Rijksweg 107-117, the NPR compliant bilinear-curve are derived from figure 36 and 37 of par. 7.2.2 of [VIIA 2019a]. The properties of the bilinear-curves and a visual representation of the latter are summarized in, respectively Table A.7 and Figure A.20. By comparing the bilinear curves in Figure A.20 and Figure A.19 it can be observed that the normalized base shear of the bilinear curves is larger compared to the backbone curves computed. This difference in normalized base shear can be explained by the different mass used (effective mass < dynamic mass). The difference in collapse displacement is related to the adoption of the transformation factor $\Gamma$.

Table A.7 Yield and near-collapse points of the bilinear curves of Rijksweg 107-117 and corresponding total damping.

| **Building** | **Ref.** | $d_y$ $[mm]$ | $d_u$ $[mm]$ | $a_u$ $[g]$ | $\xi_{sys}$ [%] |
|---|---|---|---|---|---|
| Rijksweg 107-117 (long.) | [VIIA 2019a] | 9.8 | 45.0 | 0.342 | 15.2 |
| Rijksweg 107-117 (trans.) | [VIIA 2019a] | 9.75 | 32.33 | 0.387 | 18.6 |

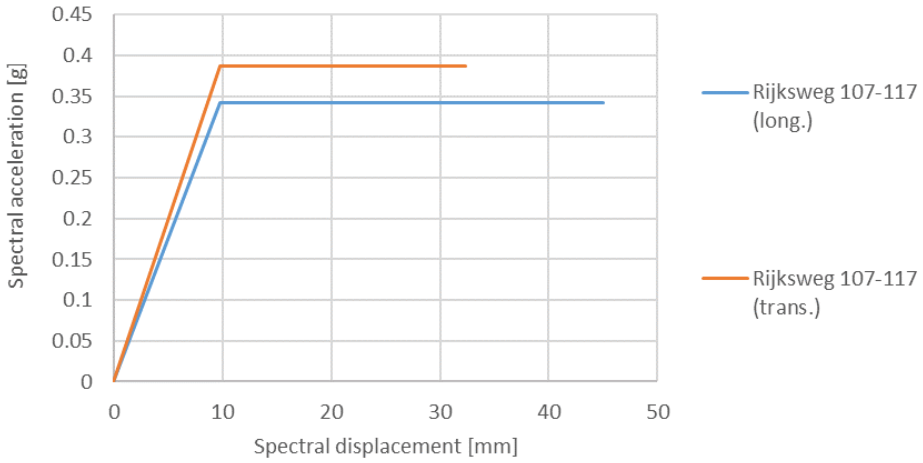


Figure A.20 Bilinear curve for both direction of Rijksweg 107-117 in [VIIA 2019a].

### *A.4.5 Safety assessment according to NPR 9998*

The assessment described in this section is based on the global performance of the building using acceleration-displacement response spectra (ADRS) which are compared against the bilinear curve in Table A.7. The compliance of the bilinear curve is checked for cell of the NEN webtool and for each curve the performance

indicator, i.e. the ratio between the building capacity and the seismic demand at the performance point. Figure A.21 shows the bilinear curve against all the elastic and inelastic (damped) ADRS while Figure A.22 presents the distribution of the performance indicators for Rijksweg 107-117 over the NEN grid. The minimum performance indicators correspond to 3.22 and 2.83 for the longitudinal and transverse directions respectively. Since the bilinear curve is compliant to all the ADRS curves, none of the NEN cells are unsafe with respect to the global in-plane failure of the buildings.

In addition, also the local failure mechanisms, and especially the out-of-plane (OOP) failure of the walls, must be assessed. For Rijksweg 107-117, the assessment with respect to out-of-plane mechanisms is performed in [VIIA 2019a] using an NLKA analysis. The analysis didn't show collapses of load-bearing walls. Non-structural constructive elements (NSCEs) are also assessed in [VIIA 2019a] which reports the OOP failure of the outer leaf of the gable walls at attic level. Since the OOP failure affects non-load bearing walls, accounting for the local out-of-plane failure mechanism would not modify the outcomes of the vulnerability assessment as presented in this section. The NLKA analyses were performed using a response spectrum for which the maximum spectral acceleration was 0.38 g. No OOP failure of load-bearing walls was observed in these analyses.

Since the maximum spectral acceleration of the v6-t5 NEN webtool spectra is 0.45g, no final conclusion can be drawn for the cells above 0.38g (312 cells) based on the NLKA analyses presented above. However, as observed later in section A.6, no out-of-plane collapse was observed in the available NLTH analyses before global in-plane collapse occurs. This is a strong indication that OOP mechanisms are not governing the collapse of Rijksweg 107-117.

Based on these considerations none of the NEN cells are expected to be unsafe with respect to all failure mechanisms (both in-plane and out of plane) of the buildings.

Since the assessments performed on Rijksweg 119-129 are exactly as Rijksweg 107-117, similar conclusions can be drawn about the compliance of the building to the safety assessment according to the NPR 9998 for both in-plane and out-of-plane collapses.

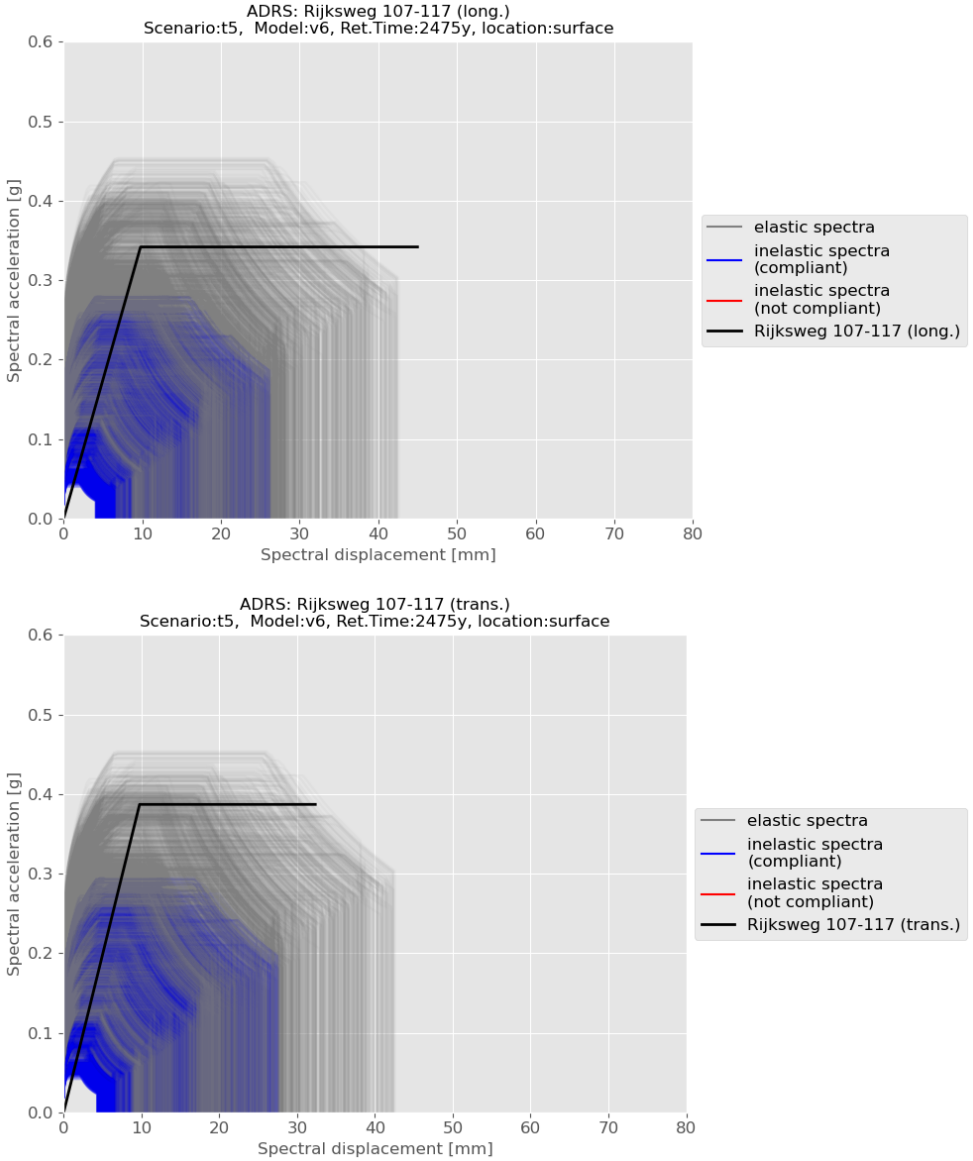


Figure A.21 ADRS spectra (elastic in grey and inelastic in blue) against the bilinear curves of Rijksweg 107-117 (solid black line): longitudinal (top) and transverse (bottom) directions.

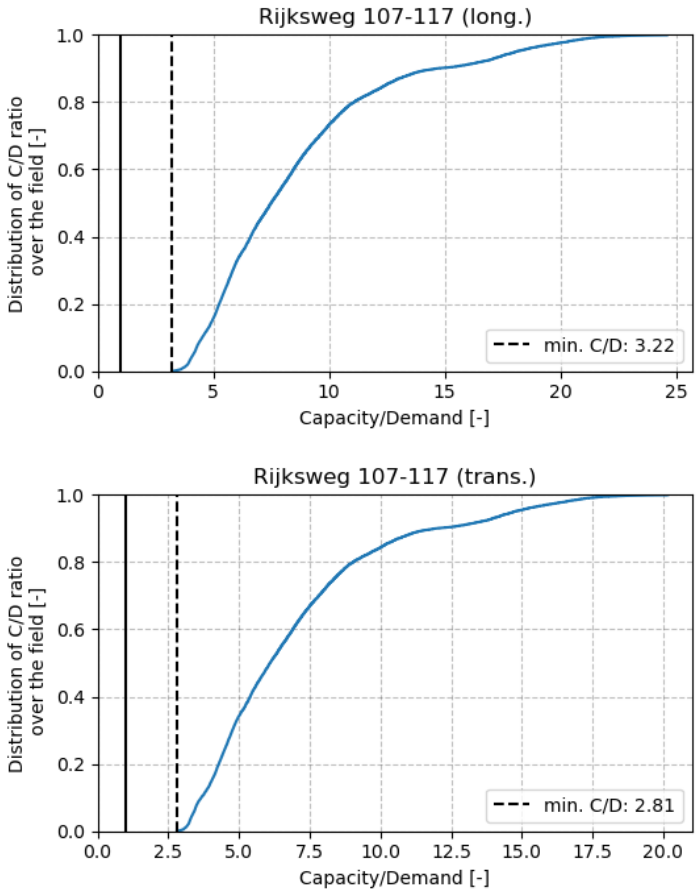


Figure A.22 Distribution of the performance indicators (ratio between capacity and demand) over the NEN grid for the bilinear curve of Rijksweg 107-117 in the longitudinal (top) and transverse (bottom) directions. The capacity over demand ratio of 1 is indicated with a black vertical solid line while the minimum ratio computed from the ADRS curves is indicated with a black vertical dashed black.

## A.5 De Helling 2-6 and Jachtlaan 16-18B

### *A.5.1 Description*

De Helling 6-8 and Jachtlaan 16-18B is a basement terraced apartment building made of a basement, three storeys and an attic (see Figure A.23). The building, divided in two compartments, is characterised by URM cavity walls, concrete floors and internal load-bearing URM walls.

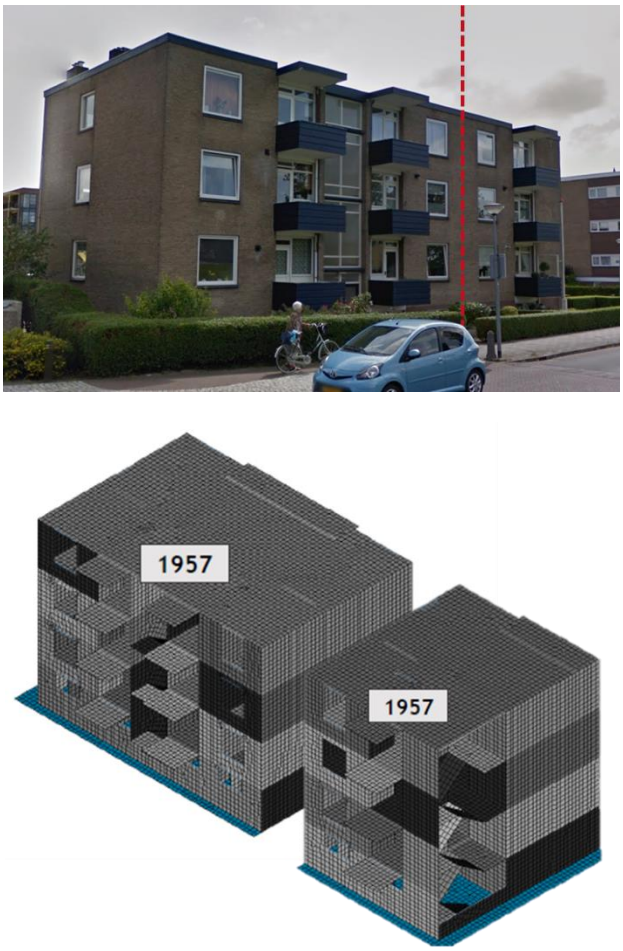


Figure A.23 Top: Side view of Jachtlaan (left-side of the red line) and De Helling (right-side of the red line), taken from Google Street View); Bottom: FEM model of Jachtlaan (left-hand block) and De Helling (right-hand block) adopted in [VIIA 2020].

The concrete floors on the first and second floors are not continuous over the two compartments and they are disconnected. Instead, the foundation plate, which is also the floor in the basement, the roof and the ground floor span through the compartments.

Due to discontinuity in the floors on the first and second floors at the location of the compartment separation two separate models were analyzed in DIANA in [VIIA 2020]. At the places where the compartments are connected to each other, i.e. at the edges of the floors where they actually run through, a boundary condition has been applied that blocks rotation around the relevant axis.

Only the primary and secondary seismic elements are modeled, while non-seismic constructive elements (NSCE, such as the outer cavity wall of the facade, chimneys, non-load-bearing walls, free-standing walls and parapets on the balcony) have not been modelled since they do not contribute to the stability of the building and are assessed separately. The mass of these elements is included in the model.

The building has a regular structure with stability walls in two directions, which is beneficial for the seismic response. The building contains only sand-lime brick walls

and reinforced concrete floors. The facades are made up of cavity walls, whose inner leaf made of sand-lime brick masonry guarantees the stability of De Helling and Jachtlaan.

Figure A.24 shows the wall configuration on the basement and at ground-floor level. The building has a regular plan and a regular wall configuration across the height, except for the basement, where the openings are smaller and a larger number of 200mm URM walls is present compared to the upper floors. The building presents URM load-bearing walls spanning along the longitudinal and transverse direction (respectively X and Y in Figure A.24).

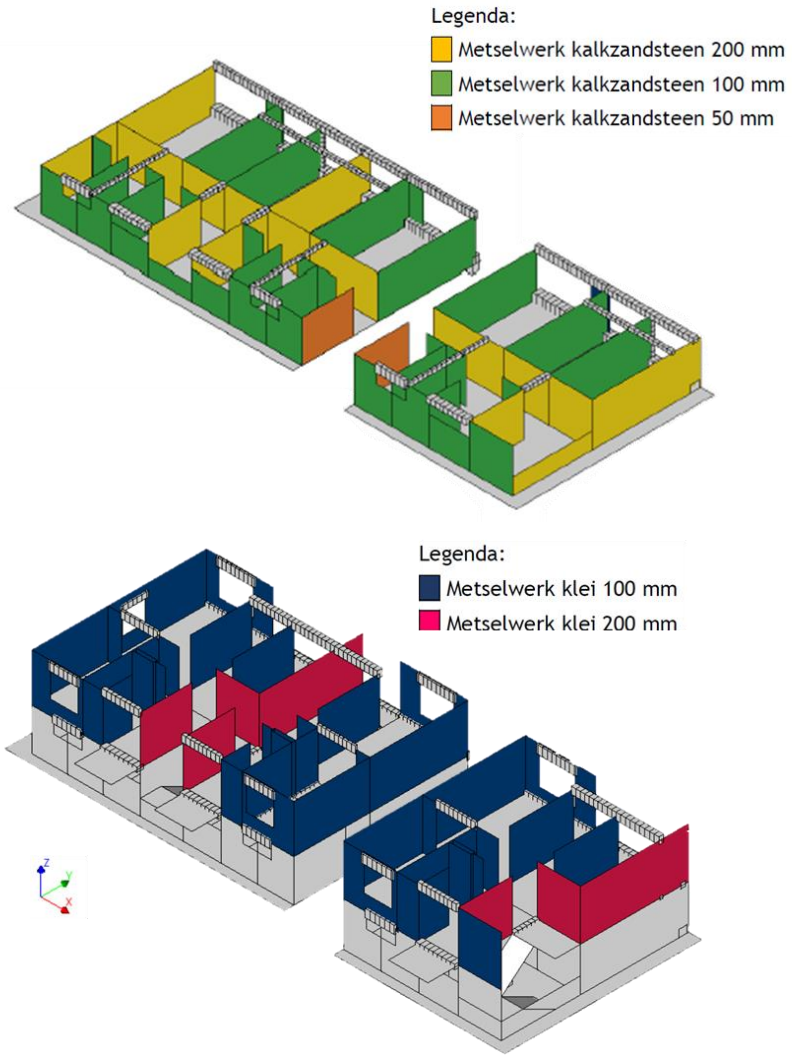


Figure A.24 Wall configuration at the basement (top) and the first floor (bottom) of the FEM model of Jachtlaan (left) and De Helling (right) in [VIIA 2020].

For both Jachtlaan and De Helling, the NLPO analyses were carried in both longitudinal and transverse directions. The out-of-plane capacity of the walls is checked using non-linear kinematic analyses (NLKA).

The analyses are stopped when the drift limits at near collapse recommended in NPR 9998 are exceeded at one of the floor levels. Since progressive collapse is not

modelled explicitly as in [ARUP 2019], the real collapse displacement of the building investigated in [VIIA 2020] is expected to be larger than the one reported and shown by the capacity curves, although it is not possible to quantify how much larger. For both buildings, the FE package DIANA FEA was adopted to perform the NPLO analyses.

### *A.5.2 Backbone from NLPO analyses*

The NPLO analyses provided in [VIIA 2020] are compared against the capacity curves (the so-called backbone curves) of the index buildings of METSELWERK-D. Figure A.25 shows the capacity curves of Jachtlaan and De Helling in both transverse and longitudinal directions, since the presence of load-bearing walls in both directions does not allow to identify a-priory the governing (weaker) direction. The post-peak behaviour of Jachtlaan and De Helling was not investigated, thus the real ductility of the building is unknown.

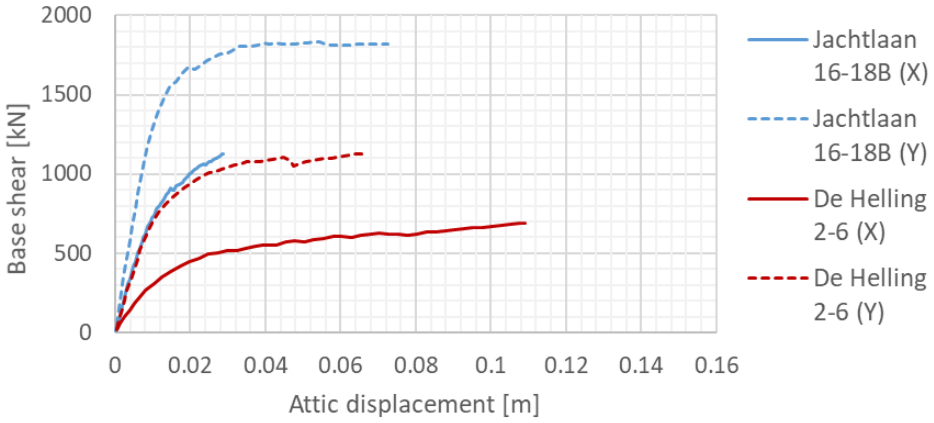


Figure A.25 Capacity curves extrapolated from [VIIA 2020] for Jachtlaan (blue) and De Helling (red) for longitudinal (X, solid) and transverse (Y, dashed) directions.

To compare the curves of Jachtlaan and De Helling with those of the index buildings Schuitenzandflat and Koeriersterweg, the base-shear capacity has to be normalized by the effective weight of the building, obtained by the product between the effective mass ($m_e$) and the gravity acceleration ($g$). Similar to Rijksweg 107-117B, the normalization was performed using the total dynamic weight reported in [VIIA 2020] because it was not possible to determine precisely the effective mass of the building. This is a conservative assumption since using the effective weight would lead to a larger normalized base shear capacity. The adopted dynamic mass related to each capacity curve presented in Figure A.25 is summarized in Table A.8.

Table A.8 Dynamic weight adopted from the analyses to normalize the base-shear capacity of the capacity curves.

| Curve | Dynamic weight [kN] |
|---|---|
| De Jachtlaan 16-18B (X) | 3896.6 |
| De Jachtlaan 16-18B (Y) | 3896.6 |
| De Helling 2-6 (X) | 2307.4 |
| De Helling 2-6 (Y) | 2307.4 |

Figure A.25 shows the capacity curves in Figure A.26 after being scaled by the dynamic weight together with the Schuitenzandflat and Koeriersterweg.

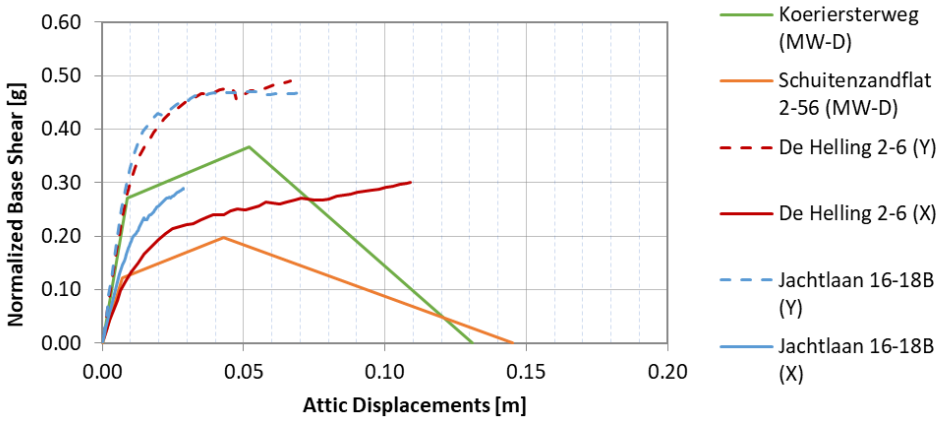


Figure A.26 Normalized capacity curves obtained from [VIIA 2019a] compared against the backbone curves selected for METSELWERK-D (MW-D).

Given that the wall configuration of Jachtlaan and De Helling is similar in both transverse and longitudinal direction, the corresponding backbone curves should also correspond. From the figure, the following is observed:

- The backbone curves in the transverse direction (Y) of Jachtlaan and De Helling overlap, which means that the buildings have a substantially equivalent behaviour in the transverse direction. This matches well with the observation on the floor configurations of the two parts of the building.
- The longitudinal direction (X) appears to be the governing direction for both buildings. The maximum displacement for Jachtlaan is smaller compared to De Helling due to the exceedance of the drift limits prescribed in NPR 9998. Given that the wall configuration is similar, the real ductility of Jachtlaan is expected to be larger than the one obtained from the reported push-over curves, and more in line with the backbone curve obtained for De Helling in the longitudinal direction. However, since explicit collapse is not modelled, the real collapse displacement is expected to be larger.
- The backbone curves of Jachtlaan and De Helling are positioned in between the ones of Koeriersterweg and Schuitenzandflat index buildings.

### *A.5.3 Collapse mechanisms*

The global collapse mechanisms observed in [VIIA 2020] relates to in-plane collapse mechanisms. Additionally, the assessment performed via NLKA showed that all the load-bearing walls (thickness 100 and 200mm) meet the out-of-plane failure criteria. For non-structural construction elements, the outer leaf of the URM cavity walls and partition walls are assessed suing semi-probabilistic analysis (see NPR9998: 2020, par. 4.3.6.3) while chimneys and parapets are assessed with generic risk analysis (see NPR9998: 2020, appendix H). The capacity of the NSCE elements were all found to be compliant to the NPR9998 assessments.
It is concluded that the full-collapse of Jachtlaan and De Helling is related to a shear failure of the load-bearing walls, although the progressive collapse was not modelled.

### *A.5.4 Definition of the equivalent bilinear curves (according to NPR 9998 [NPR, 2020])*

For Jachtlaan and De Helling, the NPR-compliant bilinear-curves are derived respectively from figures 52 and 53 of par. 7.2.1.2 and figures 80 and 81 of par. 7.2.2.2 in [VIIA 2020]. The properties of the bilinear-curves and a visual representation of the latter are summarized in Table A.9 and Figure A.27, respectively. By comparing the bilinear curves in Figure A.27 and Figure A.26, good agreement between the curves in the longitudinal (weak) direction is observed in terms of spectral acceleration while Jachtlaan bilinear curve presents a smaller collapse displacement compared to De Helling. The difference in collapse displacement between the curves presented in Figure A.27 and the corresponding curves in Figure A.26 is related to the adoption of the transformation factor $\Gamma$.

Table A.9 Yield and near-collapse points of the bilinear curves of Jachtlaan 16-18 and De Helling 2-6 and corresponding total damping.

| **Building** | **Ref.** | $d_y$ $[mm]$ | $d_u$ $[mm]$ | $a_u$ $[g]$ | $\xi_{sys}$ [%] |
|---|---|---|---|---|---|
| Jachtlaan 16-18 (long.) | [VIIA 2020] | 9.6 | 20.9 | 0.324 | 15.2 |
| Jachtlaan 16-18 (trans.) | [VIIA 2020] | 6.7 | 54.2 | 0.374 | 20.0 |
| De Helling 2-6 (long.) | [VIIA 2020] | 18.1 | 79.3 | 0.333 | 20.0 |
| De Helling 2-6 (trans.) | [VIIA 2020] | 10.83 | 49.4 | 0.520 | 20.0 |

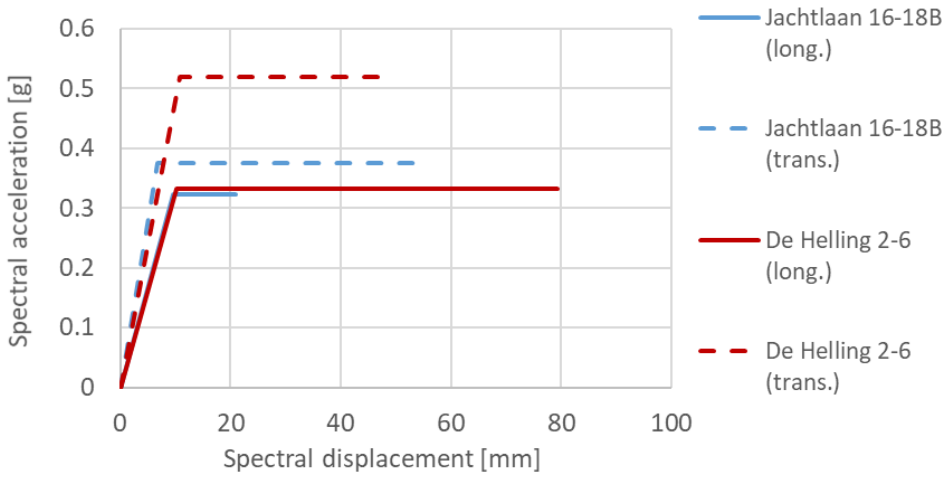


Figure A.27 Bilinear curve for both direction of Jachtlaan 16-18B and De Helling 2-6 from [VIIA 2020].

### *A.5.5 Safety assessment according to NPR 9998*

The assessment described in this section is based on the global performance of the building. The acceleration-displacement response spectra (ADRS) are compared against the bilinear curve in Figure A.27 according to the procedure reported in Annex G of NPR 9998:2020. The compliance of the bilinear curve is checked for

each cell of the NEN webtool and for each curve the performance indicator is defined, i.e. the ratio between the building capacity and the seismic demand at the performance point (equivalent to the capacity over demand ratio). Figure A.28 and Figure A.30 show the bilinear curve against all the elastic and inelastic (damped) ADRS for respectively Jachtlaan 16-18 and De Helling 2-6. Since the bilinear curve is compliant to all the ADRS curves, none of the NEN cells are unsafe with respect to the global in-plane failure of the buildings. Figure A.29 and Figure A.31 present the distribution of the performance indicators over the NEN grid for, respectively, Jachtlaan 16-18 and De Helling 2-6. The minimum performance indicators are 1.37 and 6.56 for Jachtlaan in the longitudinal and transverse directions respectively. For De Helling, minimum performance indicators are 2.92 and 5.23 in the longitudinal and transverse directions, respectively. It should be noted that, as observed already for the backbone curves presented for De Helling and Jachtlaan, the ductility of Jachtlaan in the longitudinal direction is a conservative estimate when compared to the ductility of De Helling in the same direction.

In addition to the assessment of the global performance of the building, also the local failure mechanisms, and especially the out-of-plane (OOP) failure of the walls, must be assessed. For Jachtlaan 16-18 and De Helling 2-6, the assessment with respect to out-of-plane mechanisms is performed in [VIIA 2020] using NLKA. The analysis does not return any collapse of the load-bearing walls. Non-seismic structural elements are also assessed in [VIIA 2020], and the safety criteria are met by all the elements. It is concluded that OOP local mechanisms do not modify the outcomes of the vulnerability assessment as presented in this section. The NLKA analyses were performed using a response spectrum for which the maximum spectral acceleration was 0.38 g. No OOP failure of load-bearing walls was observed in these analyses.

Since the maximum spectral acceleration of the v6-t5 NEN webtool spectra is 0.45g, no final conclusion can be drawn for the cells above 0.38g (317 cells) based on the NLKA analyses presented above. However, as observed later in section A.6, no out-of-plane collapse was observed in the available NLTH analyses before global in-plane collapse occurs. This is a strong indication that OOP mechanisms are not governing the collapse of Jachtlaan 16-18 and de Helling 2-6.

Based on these considerations none of the NEN cells are expected to be unsafe with respect to all failure mechanisms (both in-plane and out of plane) of the buildings.

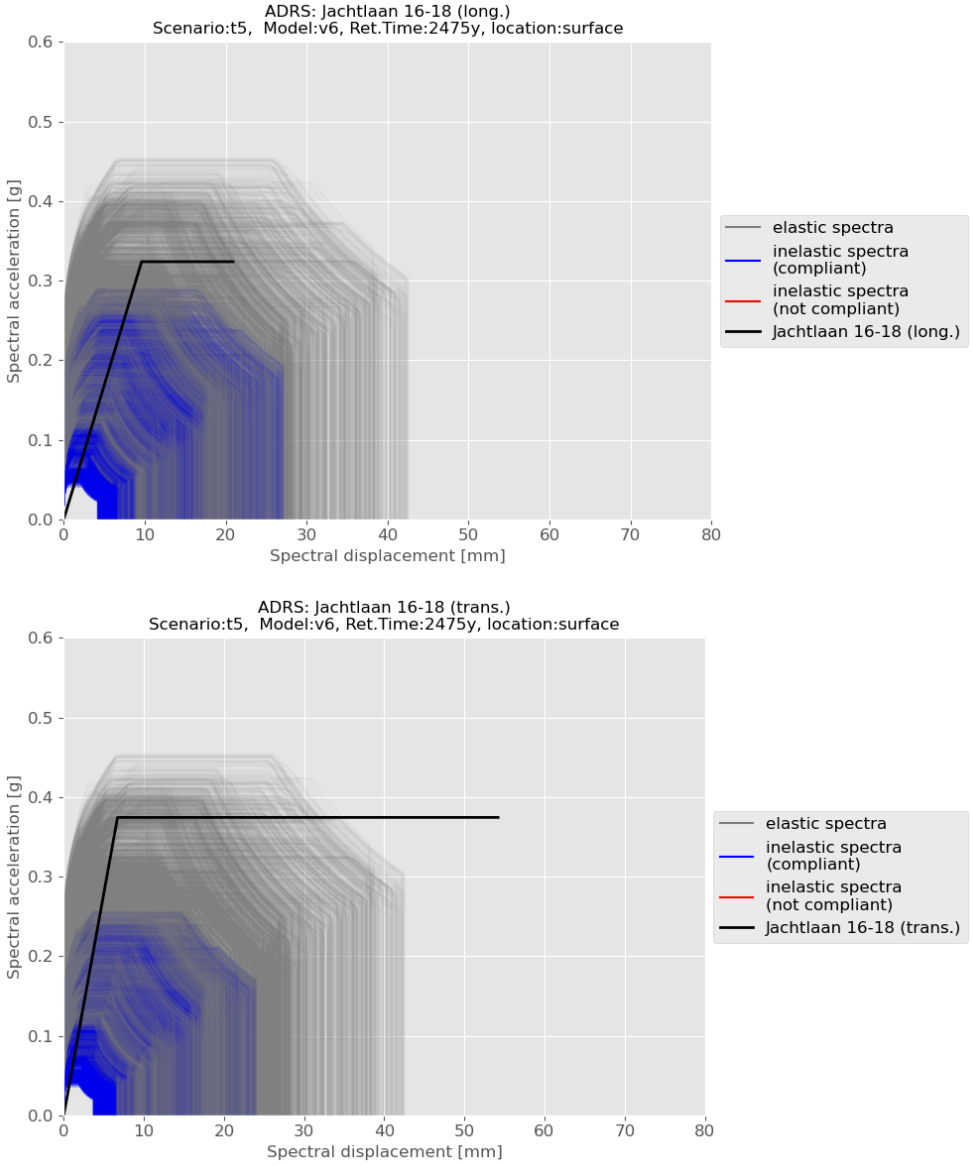


Figure A.28 ADRS spectra (elastic in grey and inelastic in blue) against the bilinear curves of Jachtlaan 16-18B (solid black line): longitudinal (top) and transverse (bottom) directions.

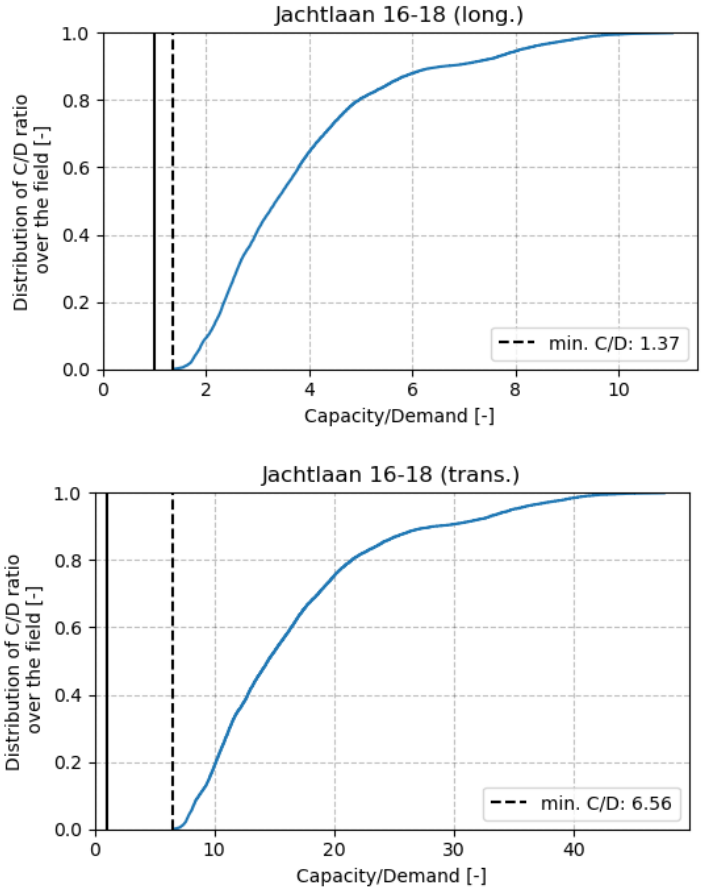


Figure A.29 Distribution of the performance indicators (ratio between capacity and demand) over the NEN grid for the bilinear curves of Jachtlaan 16-18B in the longitudinal (top) and transverse (bottom) directions. The capacity over demand ratio of 1 is indicated with a black vertical solid line while the minimum ratio computed from the ADRS curves is indicated with a black vertical dashed black.

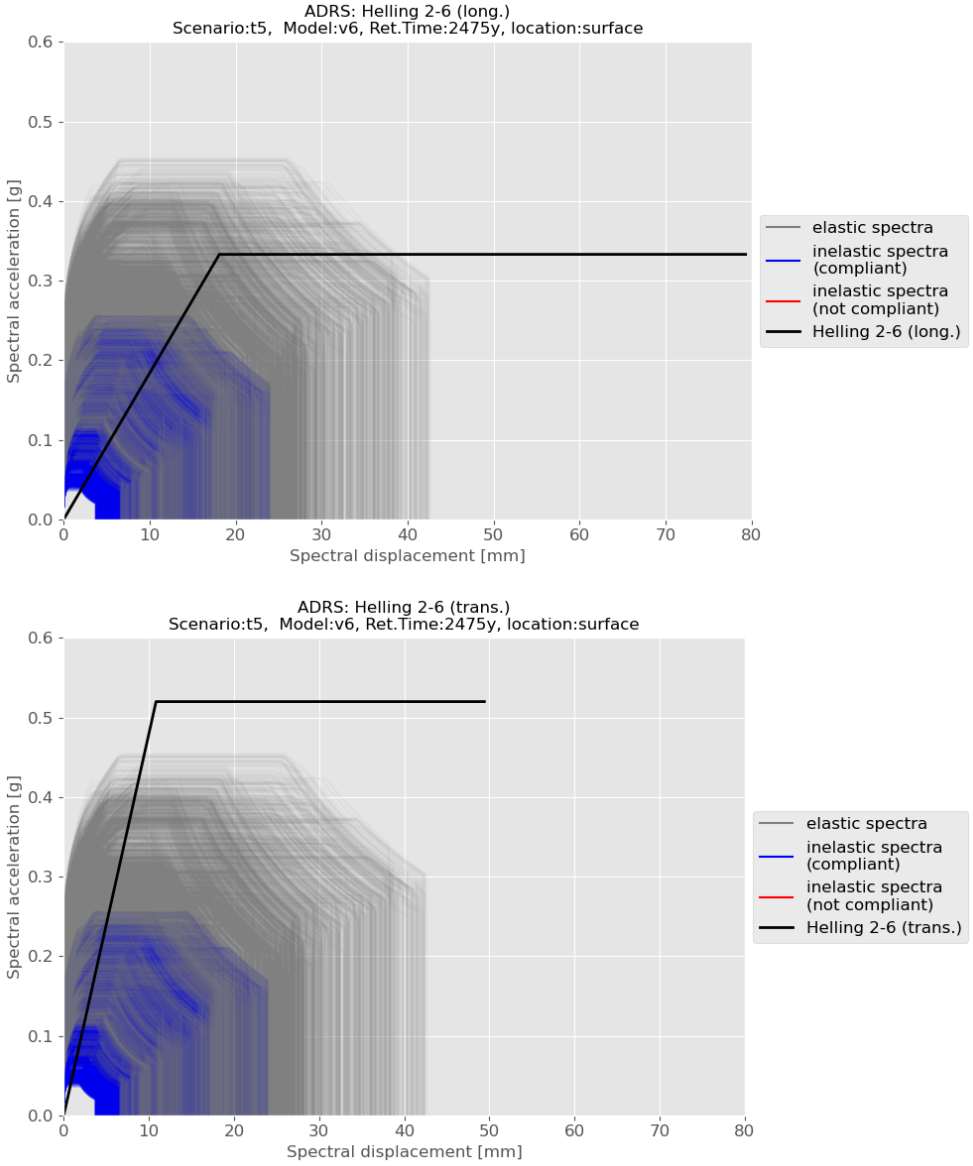


Figure A.30 ADRS spectra (elastic in grey and inelastic in blue) against the bilinear curves of De Helling 2-6 (solid black line): longitudinal (top) and transverse (bottom) directions.

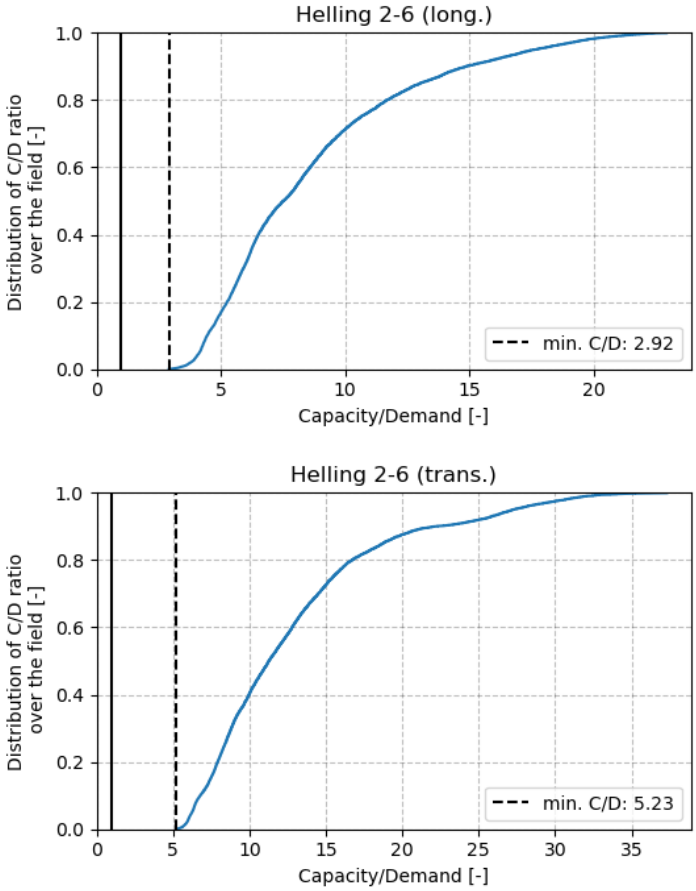


Figure A.31 Distribution of the performance indicators (ratio between capacity and demand) over the NEN grid for the bilinear curves of De Helling 2-6 in the longitudinal (top) and transverse (bottom) directions. The capacity over demand ratio of 1 is indicated with a black vertical solid line while the minimum ratio computed from the ADRS curves is indicated with a black vertical dashed black.

## A.6 Additional assessments on buildings assigned to METSELWERK-D using NLTHA

This section summarizes the results of the NLTHA studies for three buildings belonging to METSELWERK-D carried out based on NPR 9998: 2015, see section A.1. These studies use ground motion records for a specific location to assess the global performance of the building, and as such they can't be used to derive backbone curves, nor can the results be used to check compliance of a building against the webtool, version v6, period t5, the hazard used in the risk evaluation of METSELWERK-D.

The ground motions adopted (as prescribed by NPR 9998:2015) present PGA values significantly higher than those defined in the NEN webtool v6-t5 (used in this study). Therefore, the conclusions that can be drawn from these studies are limited: the outcomes of these NLTHA can be used to identify the prevailing failure mechanisms, and determine whether out-of-plane failure of structural and non-structural elements is expected. The NLTHA also allows to check whether the outcomes of the assessment are consistent with that obtained according to the typology-based assessment.

The list of the additional addresses is provided in Table A.10 together with the NPR version adopted for the analyses and the maximum PGA of the records

Table A.10 Additional addresses of buildings belonging to METSELWERK-D.

| Address | Analysis type | PGA (g) | NPR version | Ref. |
|---|---|---|---|---|
| De Rank 7-11B | NLTHA | 0.7 | 2015 | [Arup 2017e] |
| Abel Eppensstraat 15-69 | NLTHA | 0.7 | 2015 | [Arup 2017c] |
| Georg van Saksenlaan 27-37B | NLTHA | 0.7 | 2015 | [Arup 2017d] |

### *A.6.1 De Rank 7-11B*

Figure A.32 Side view of De Rank 7-11.

The building, a four-storey apartment building constructed in 2008 shown in Figure A.32, was analyzed by Arup [Arup, 2017e]. The structure consists of clay and calcium silicate bearing walls supporting filigree slabs for the first, second, and third floors, and precast hollow core slabs at the ground and roof levels. The foundations are a series of reinforced concrete foundation beams supported by concrete piles. The NLTHA performed on the as-built construction indicate that the lateral support system for the roof is inadequate, and the failure of the roof leads consequently to total collapse of the building. Additional NLTHA are performed after adding preliminary retrofits for the lateral support system of the roof; such analyses show further deficiencies:

- failure of a calcium silicate wall in the third floor of the stairwell;
- failure of cavity parapet walls and outer leaves;
- failure of foundation piles.

Besides, the partition walls are made of Ytong aerated lightweight concrete blocks and are not properly connected at the top to the upstanding floor (the walls have a gap on top that is filled with polyurethane). Such walls have not been modelled for De Rank, but they have investigated by ARUP in previous buildings with similar features resulting in out of plane failure in all floors.

It is then concluded that loadbearing walls are not vulnerable in the out-of-plane direction, whereas the non-loadbearing walls (partition walls and outer leaves) are predicted to collapse.

### *A.6.2 Abel Eppensstraat 15-69*

Figure A.33 Side view (left, from Google street view, in 2009) and particular of the entrance (right, left, from [Arup 2017d], in 2014) of Abel Eppenstraat 15-69.

The building, presented in Figure A.33, is a four-storey apartment building constructed in 1970,analyzed by Arup [Arup, 2017d]. The main structure consists of clay masonry outer leaf walls, calcium silicate inner leaf walls and calcium silicate bearing walls. The foundation is made of precast concrete piles connected to concrete grade beams. The building largely resembles the building adopted in the case study of [Noortman, 2019]. Based on the available material it is assumed that the building studied by [Noortman 2019] is Abel Eppensstraat 71-125. Both analyses are used in this study because they are complementary.

The NLTHA predict the complete collapse of the main structure caused by inadequate strength in the longitudinal direction of the building. Especially, the most significant damage occurs at the top of the longitudinal walls. The failure of the longitudinal resisting system leads, as a consequence, to the collapse of the transversal walls due to out-of-plane bending triggered by the very large imposed deformations (once more, due to the failure of the longitudinal resisting system) and eventually to the collapse of the supported floors and roof.
Additionally, also the following deficiencies are identified:

- collapse of the stairwells;
- failure of cantilever gallery and balcony beams;
- failure of the existing piles;
- collapse of the clay brick masonry outer leaves onto egress paths.

Finally, similarly to De Rank, the partition walls are not modelled. However, the lack of connection at the top leads likely to the collapse of such walls.

The report highlights that the collapse of the walls in the out-of-plane direction occurs only as a consequence of the collapse of the longitudinal piers for in-plane loading. In other words, the local out-of-plane failure of the loadbearing walls is not critical in itself. On the opposite, the non-loadbearing walls (partition walls and outer leaves) are predicted to collapse.

### *A.6.3 Georg van Saksenlaan 27-37B*

Figure A.34 Side view Georg van Saksenlaan 27-27B.

The building, which is shown in Figure A.34, is a four-storey apartment building constructed in 1965, analyzed by Arup [Arup 2017c]. The load-bearing structure consists of longitudinal and transverse masonry shear walls. The foundation is composed of perimeter reinforced concrete foundation beams which sit on a reinforced concrete slab on grade.
The NLTHA do not predict the complete collapse of the building. However, the following deficiencies that make the as-built constructions not compliant to the NPR 9998:2015 are identified:

- Collapse of part of the primary seismic walls, especially at the first storey.
- Damage to the outer leaves of the masonry façade, including above the front door (with consequent possible fall of debris on the egress path).
- Failure of the chimney.
- Failure of the primary seismic walls on the stairway structure on the top floor leading also to the failure of the landing slabs which are part of the egress path.

The loadbearing walls are therefore not vulnerable for out-of-plane loads, whereas the collapse of part of the veneers of the masonry façade is predicted.

### *A.6.4 Summary*

The outcomes of the NLTHA presented above are summarized as follows:

- All the buildings have been analysed based on NPR9998:2015. In this NPR, significantly stronger ground motions than those currently considered (webtool, v6 - t5) were applied.
- All cases show that insufficient in-plane capacity of the structure dominates the failure mechanism.
- No out-of-plane collapse of loadbearing walls is reported.
- Non-loadbearing walls such partition walls and outer leaves of cavity walls may undergo out-of-plane failure.

Such outcomes are in line with those presented in sections A.3, A.4 and A.5: out-of-plane failure may be critical for non-loadbearing walls, whereas the loadbearing walls fail in the in-plane direction.

## A.7 Results

To increase the confidence in the fragility and consequence model proposed for METSELWERK-D, TNO and TU Delft investigated the availability of 'bottom up' NPR 9998 studies on buildings that can be assigned to METSELWERK-D. From the material made available by NCG, six TVAs were suitable for the analyses and were studied in detail. In addition the findings of the TU Delft Master thesis [Noortman, 2019], were studied. The analyses are listed in Table A.1.

From the 4 buildings analysed using NLPOs, backbone curves for the most vulnerable loading condition were computed. These backbone curves are compared to the backbone curves of the two index buildings of METSELWERK-D in Figure A.35.

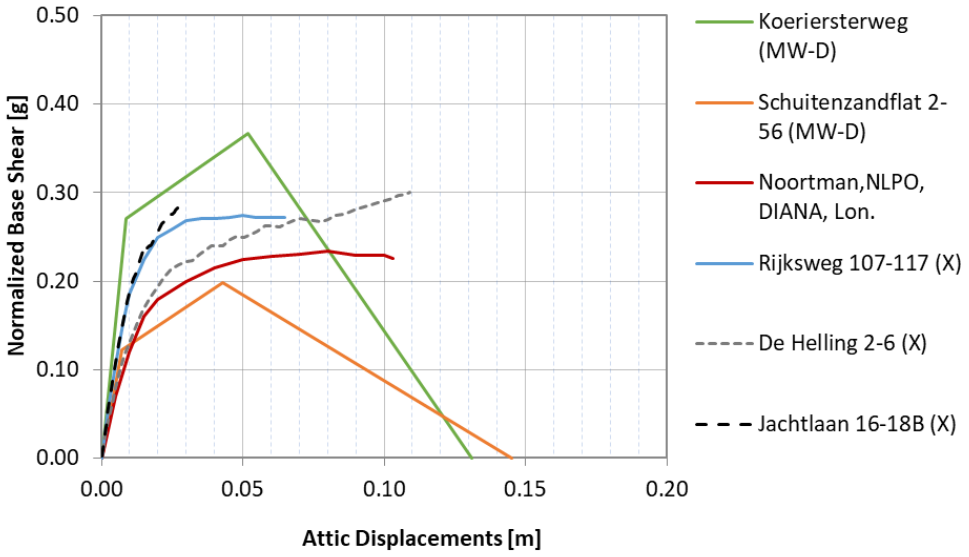


Figure A.35 Normalized capacity curves obtained from [VIIA 2019a, 2020] and [Noortman, 2019] against the backbone curves selected for METSELWERK-D (MW-D).

All the normalized base shear forces of the considered buildings are comprised between the values of the two index buildings, which represent therefore a lower and upper bound for the selected cases. It should be noted that the NC displacement capacity of the analyzed buildings is usually lower than that reported for the two index buildings, but this mainly depends on the application of the drift limits recommended in Annex F and G of NPR 9998, which do not correspond to the expected (median) displacement at collapse of the building. For this reason, the best estimate NC displacements of the buildings will be larger than the values reported in Figure A.35, although it is not possible to quantify how much larger.

With respect to the collapse mechanisms, the four buildings are characterized by large global in-plane deformations, although the analyses are not performed up to near collapse of the building. Rocking of the piers is observed and, in the case of the building studied in [Noortman, 2019], this is concluded by shear splitting failure which leads to a drop of resistance of the piers. This is similar to what was

observed in the experimental tests performed in 2016 at TU Delft [Esposito et al., 2018]. No out-of-plane failure of the load-bearing walls is observed for the three buildings analyzed using NLTHA.

The safety of the buildings presented in Figure A.35 has been assessed according to the procedure reported in appendix G of NPR 9998: 2020 for each cell of the NEN webtool. The assessment shows that the buildings are compliant in every of the NEN cells with respect to the global in-plane failure of the buildings. It was shown in 4.3 to 4.6 that in plane failure occurs before out of plane failure of loadbearing walls so the in plane capacity over demand ratios are governing. The resulting capacity of demand ratios for the analysed buildings are shown in Table A.11.

Table A.11 C/D ratio's for the 'bottom up' analysed buildings

| **Building** | **Minimum C/D ratio in the Groningen region covered by the NEN webtool for the governing building direction** |
|---|---|
| Noortman, 2019 | 2.04 |
| Jachtlaan 16-18B (long.) | 1.4 |
| De Helling 2-6 (long.) | 2.92 |
| Rijksweg 107-117B (long.) | 3.22 |

In conclusion, the performed assessment shows that the buildings are all compliant to NPR 9998:2020 in every cell of the NEN webtool.

# B Ligging referentiegebouwen in Groningse gebouwenpopulatie

## B.1 Inleiding

In deze bijlage wordt toegelicht welke overwegingen ten grondslag hebben gelegen aan de keuze van de referentiegebouwen, zodanig dat deze zo goed mogelijk aansluiten bij de gebouwen die voorkomen in de Groningse gebouwenvoorraad. Het vervolg van deze bijlage is in het Engels.

## B.2 Introduction

For every typology, the risk calculation by the TNO model chain combines the hazard resulting from seismic activity with a fragility and consequence model, which describe, respectively, the vulnerability of the building stock to given hazard, and the exposure of the people to risk. In the risk calculation different limit state conditions are used to calculate the individual risk of dying for a person who is continuously present within or near a building and who is unprotected. The fragility functions describe the probability of exceeding a given limit state condition of a certain building for the intensity measure of the ground motion. This fragility function includes the mean response for a certain ground motion intensity as well as the record-to-record variability for different signals of the same intensity. Additional to the record-to-record variability, the building-to-building variability and model uncertainty (both due to lack of accurate information and limited accuracy of the models) are accounted for separately.

The fragility functions adopted in the typology approach and the sensitivity study follow from the approach outlined in the main TNO report [TNO, 2021a].

The structural behaviour is simulated using accurate non-linear time-history analyses (NLTH) on a multi-degree-of-freedom (MDOF) model of the structure (which represents the median building of the typology) subjected to 11 ground motion records.

The choice that led to the definition of the index buildings (index buildings are reference buildings for the fragility development) was based on a study of the building stock performed by Arup, which developed and updated an exposure database (EDB) in [Arup 2016b, Arup 2017b, 2019a and 2019d]. The EDB contains the location, structural characteristics and exposed population (inside and outside) of over 250,000 buildings inside and within 5km of the Groningen gas field. The EDB study makes use of numerous building data sources, including physical and desktop inspection data, open and licensed data related to the geometry, function and building construction attributes per building, and additional processed building data.

In particular, the EDB employs the available data to assign to each building so-called GEM taxonomy strings summarizing the main features. Backgrounds on these GEM taxonomy strings can be found in [Brzev et al, 2013]. The attributes that are included in the GEM string are outlined in Table B.1. The information available from the exposure database allows to:

- Cluster the Groningen building stock into typologies.
- For each typology, extract the distribution and median values of the building properties, as a basis to define a median building within each typology.

Table B.1 Attributes included in the GEM taxonomy string for the Exposure database [Arup 2019d]

| Parameter | Description |
|---|---|
| Structural layout | Classification of Buildings according to their main geometric features (characteristic width and length of the maximum enclosed rectangle within a Building ID's footprint and the average height of a Building IDs). |
| Structural materials and Lateral load-resisting system | The structural system and material that provides lateral resistance against horizontal loads. This is specified for the primary and secondary direction of the building. |
| Presence of external walls | Presence of cavity walls |
| Floor material | Material that constitutes the majority of the floors in the building |
| Number of storeys | Range of number of storeys above ground |
| Presence of irregularities | Presence of vertical structural irregularity (e.g. large opening at ground floor level, presence of a garage at the ground floor or a soft storey) |

Using the available data, Arup clustered the building stock into typologies characterized for the rest of the buildings. A structural system inference was applied to determine the likelihood of each building belonging to one of the defined structural systems.

## B.3 Representativeness of the selected index (median) buildings

The index (or median) building of a given typology is a building for which the structural and geometrical properties and strength can be considered the median of the considered typology.

The selection of index buildings for fragility development builds on a series of reports on the fragility and consequence models, starting from [Crowley et al, 2015]. In par. 3.8 of this document, also referred to as v2 fragility and consequence model:

"*index buildings are assumed to represent the median capacity of a given building typology. The validity of this assumption for the URM buildings in particular should be studied during the development of the v3 fragility functions, and structural drawings for a number of index buildings of each typology are currently being collected for this purpose.*"

The representativeness of the index buildings in [Crowley et al, 2015] for the respective typologies was investigated by Arup in [Arup 2017a]. For this purpose building properties related to geometry and year of constructions were selected (see Table B.2). In the study, Arup selected some of the macro-typologies of interest and extracted for those the distribution of the selected building characteristics using 300 samples from EDB V3 [Arup 2016a]. The macro-typology concerns buildings with the same category use as described in [Crowley et al, 2015], but which are characterized by different structural systems. Finally, the distributions of the characteristics are compared to those obtained from the index buildings for the corresponding typologies.

Table B.2 Properties investigated in the representativeness study of [Arup 2016c].

| Parameter | Description |
|---|---|
| Building year | The building year provided by BAG |
| Building Height | Height of the highest point of a building's geometry from the ground level (excl. chimneys) |
| Volume | The enclosed volume within the building envelope |
| Façade Area | Sum of areas of all vertical surfaces of the building envelope. In terraced buildings and older apartments, this can include also the interfaces between adjacent units |
| Gutter Height | The distance of the lengthiest linear horizontal roof-wall connection to the ground level |
| Footprint area | Area of the building's outline polygon (e.g. as provided by BAG) |
| Presence of Gable Walls | Presence/Absence of gable walls |
| Shape in Plan | Shape type of a building's footprint (Rectangular, L-shaped, S-T-U shaped and complex) |
| Presence of Extensions | Presence/Absence of extensions extension (i.e. a flat roof extension of the main building geometry, possibly built at a later stage than the building's initial construction) |

The index buildings investigated in the Arup study are presented in Table B.3.

Table B.3 Index buildings and corresponding typologies in the Typology approach investigated in [Arup 2016b].

| Index building | Typology |
|---|---|
| Nieuwstraat 8 | Not used in [Crowley et al. 2020] |
| Kwelder 1 | METSELWERK6 |
| Type C | Not used in [Crowley et al. 2020] |
| Zijlvest 25 | METSELWERK2 |
| Julianalaan 52 | METSELWERK1 |
| Schuitenzand flat | METSELWERK-D |
| Koeriersterweg 18 | METSELWERK-D |
| De Haver | METSELWERK-F |

The study in [Arup 2016c] concludes that the index buildings for METSELWERK-D are reasonably fitting with the distribution of the typology. The index buildings adopted for METSELWERK-D were compared against the properties of a sample of 300 building belonging to class RESA, described as Residential apartment buildings in [Crowley et al, 2015] of different material (URM and RC).


Figure B.1 Comparison of the properties of the 300 samples of RESA typology of and the properties of Koeriersterweg index building.


Figure B.2 Comparison of the properties of the 300 samples of RESA typology of and the properties of Schuitenzandflat index building.

From Figure B.1 and Figure B.2 it's concluded that the rectangular (regular) shape was the most common shape observed in the sample of apartment buildings. In the sample, an even number of building with and without gable walls was observed.

It should be noted that the main structural (and dynamic) properties are already considered in the GEM taxonomy string, which includes the lateral load resisting system and the floor material. Since the exposure database doesn't provide information on more structural details (such as connection type) for the entire building stock, those cannot be investigated for representativeness.

Another study on the representativeness of the index buildings is presented in Appendix B of [Crowley et al. 2017], where the distributions of construction year, footprint area, gutter height for each of the typologies identified in [Crowley et al. 2017] were computed from the EDB V5 [Arup2017b]. This distribution can be compared to the properties of the corresponding index buildings provided in [Crowley et al. 2017] and reported in Figure B.3. [Crowley et al. 2017] also provided characteristics ranges for the aforementioned properties and provided in Figure B.4.

| Index Building Name | Year of Construction | Structural Layout | Gutter Height (m) | Footprint area ($m^2$) |
|---|---|---|---|---|
| Precast RC post and beam | N/A | WBW | 6.5 | 1880 |
| Precast RC wall-slab-wall | N/A | UBH | 5.52 | 44 per unit |
| Cast-in-place RC post and beam | N/A | WBW | 6.5 | 1880 |
| Cast-in-place RC wall-slab-wall | N/A | UBH | 5.56 | 44 per unit |
| De Haver | 1900's | WBH | 2.9 (house) 3.7 (barn) | 194 (house), 1530 (barn) |
| Solwerderstraat 55 | <1945 | UBA | 6.1 | 113 |
| Julianalaan 52 | 1950's | UBH | 5.4 | 45 per unit |
| Type C | 1970's | UBH | 2.8 | 70 per unit |
| Zijlvest 25 | 1976 | UBH | 5.5 | 53 per unit |
| Koeriersterweg 20-21 | TBD | UBH | 8.59 | 50 per unit |
| Nieuwstraat 8 | 1940s | UH | 3.0 | 70 |
| Kwelder 1 | TBD | UH | 2.75 | 98 |
| Schuitenzandflat 2-56 | TBD | BTN | 13.8 | 720 |
| Badweg 12 | 1940's | UH | 2.8 | 67 |
| Kwelder 8 | TBD | UH | 2.75 | 76 |
| Steenweg 19 | 2005 | WBW | 6.5 | 432 |
| Glulam portal frame | N/A | WBW | 4.0 | 460 |
| Beneluxweg 15 | 2001 | WBW | 3.8 | 300 |

Figure B.3 Characteristics of the index buildings selected in [Crowley et al. 2017].

| Structural System | Year of Construction | Structural Layout | Gutter Height (m) | Footprint Area ($m^2$) |
|---|---|---|---|---|
| CR+PC/LPB/CR+PC/LPB/EWN/FN/HBET:1,2 | 1980-1999 | WBW | 3.1-4 | >300 |
| CR+PC/LWAL/CR+PC/LN/EWN/FC/HBET:1,2 | 1980-1999 | UBH | 5.1-6 | 51-100 |
| CR+CIP/LPB/CR+CIP/LPB/EWN/FN/HBET:1,2 | 1960-1979 | WBW | 3.1-4 | >300 |
| CR+CIP/LWAL/CR+CIP/LN/EWN/FC/HBET:1,2 | 1960-1979 | UBH | 5.1-6 | 51-100 |
| MUR/LH/MUR/LH/EWN/FW/HBET:1,2 | <1900 | WBH | 3.1-4 | >300 |
| MUR/LWAL/MUR/LN/EWN/FW/HBET:1,2 | 1920-1939 | UBH | 4.1-5 | 51-100 |
| MUR/LWAL/MUR/LN/EW/FC/HBET:1,2 | 1960-1979 | UBH | 5.1-6 | 51-100 |
| MUR/LWAL/MUR/LN/EW/FC/HBET:1,2 | 1960-1979 | UBH | 5.1-6 | 51-100 |
| MUR/LWAL/MUR/LN/EW/FC/HBET:1,2/IRIR+IRVP:CHV | 1960-1979 | UBH | 5.1-6 | 51-100 |
| MUR/LWAL/MUR/LN/EW/FC/HBET:3,20 | 1960-1979 | UBH | 8.1-9 | 51-100 |
| MUR/LWAL/MUR/LWAL/EWN/FW/HBET:1,2 | 1920-1939 | UH | 3.1-4 | 51-100 |
| MUR/LWAL/MUR/LWAL/EW/FC/HBET:1,2 | 1980-1999 | UH | 4.1-5 | 101-150 |
| MUR/LWAL/MUR/LWAL/EW/FC/HBET:3,20 | 1960-1979 | BTN | >11 | 151-200 |
| MUR/LWAL/MUR/LWAL/EW/FW/HBET:1,2 | 1920-1939 | UH | 3.1-4 | 101-150 |
| W/LWAL/W/LWAL/EW/FW/HBET:1,2 | 1980-1999 | UH | 4.1-5 | 101-150 |
| S/LFM/S/LFM/EWN/FC/HBET:1,2 | 1980-1999 | UH | 3.1-4 | 101-150 |
| S/LFBR/W/LPB/EWN/FN/HBET:1,2 | 1980-1999 | WBW | 3.1-4 | >300 |
| S/LFBR/S/LPB/EWN/FN/HBET:1,2 | 1960-1979 | WBW | 3.1-4 | >300 |

Figure B.4 Ranges of buildings characteristics of the typologies selected in [Crowley et al. 2017].

An updated version of Figure B.4 can be found in [Crowley et al. 2020], which expands on the previous number of index buildings. This is provided in Figure B.5.

| Index Building Name | Vulnerability Class | Year of Construction | Geometric Layout | Gutter Height (m) | Footprint area ($m^2$) |
|---|---|---|---|---|---|
| Cast-in-place RC post and beam | RC2 | N/A | W | 6.5 | 1880 |
| Precast RC post and beam | PC2 | N/A | W | 6.5 | 1880 |
| CIP RC wall-slab-wall | RC3L | N/A | U | 5.56 | 44 per unit |
| Welhaak | PC3L | 1979 | U | 5.4 | 66 per unit |
| Adamistraat | PC3L | 1979 | U | 2.85 | 90 per unit |
| De Haver barn | W1 | 1900's | W | 3.7 | 1530 |
| Kwelder 8 | W3 | 1996 | U | 2.75 | 76 |
| Steenweg 19 | S1L | 2005 | W | 6.5 | 432 |
| Beneluxweg 15 | S3 | 2001 | W | 3.8 | 300 |
| De Haver barn | URM1F_B | 1900's | WC | 3.7 | 1530 |
| De Haver house | URM1F_HC | | | 2.9 | 194 |
| Molenweg 25 barn | URM1F_B | 1877 | WC | 2.49 | 140 |
| Molenweg 25 house | URM1F_HC | | | 3.16 | 243 |
| Molenweg 29 barn | URM1F_B | 1958 | WA | 2.85 | 443 |
| Molenweg 29 house | URM1F_HA | | | 2.65 | 95 |
| Eestumerweg 51 barn | URM1F_B | 1960 | WA | 2.1 | 220 |
| Eestumerweg 51 house | URM1F_HA | | | 2.75 | 69 |
| Solwerderstraat 55 | URM2L | <1945 | U | 6.1 | 113 |
| Julianalaan 52 | URM3L | 1950's | U | 5.4 | 45 per unit |
| E45 Schildwolde | URM3L | 1971 | U | 6.17 | 59 per unit |
| Wilgenbros | URM3L | 1963 | U | 5.35 | 47 per unit |
| Oostergoweg | URM3L | 1961 | U | 5.25 | 59 per unit |
| Koeriersterweg | URM3M_U | 1941 | U | 8.59 | 50 per unit |
| Drive in | URM3M_D | 1972 | U | 8.1 | 47 per unit |
| Schuitenzandflat 2-56 | URM3M_B | 1964 | B | 13.8 | 720 |
| Zijlvest 25 | URM4L | 1976 | U | 5.5 | 53 per unit |
| E45 Delfzijl | URM4L | 1966 | U | 5.35 | 61 per unit |
| Patrimoniumstraat | URM5L | 1940's | U | 2.85 | 39 per unit |
| Kwelder 1 | URM7L | 1996 | U | 2.75 | 98 |
| Badweg 12 | URM8L | 1940's | U | 2.8 | 67 |
| Dijkstraat (building A) | URM9L | <1945 | U | 7.5 | 170 |

Figure B.5 Characteristics of the index buildings selected in [Crowley et al. 2020].

## B.4 Properties of buildings assigned to METSELWERK-D

To increase the confidence in the fragility and consequence model proposed for METSELWERK-D, TNO has received assessments a number of buildings that were, at the time, assigned to METSELWERK-D by the Nationaal Coördinator Groningen (NCG). The material received consisted of Technical Strengthening Advices (Technisch Versterkings Adviezen, TVA) carried out by different consultants. The full list of TVAs received and the selection process is described in appendix C, while the comparison between the TVAs of the selected building and the index buildings is described in appendix A. The analyses also include a TU Delft Master thesis [Noortman, 2019] The characteristics of 2 of the buildings were extracted and checked against the properties of the selected median buildings. The list of building together with their properties is summarized in Table C.4

Table C.4 Properties of the buildings assigned to METSELWERK-D.

| **Building** | **Ref.** | **Gutter height** $[m]$ | **Construction year** | **Footprint area** $[m^2]$ |
|---|---|---|---|---|
| Koeriersterweg | [Crowley et al. 2020] | 8.6 | 1941 | 50 (unit). |
| Schuitenzandflat | [Crowley et al. 2020] | 13.8 | 1964 | 720 total (~85 unit) |
| Rijksweg 107-117 (long.) | [VIIA 2019a] | 10.14 | 1956 | 54 (unit) |
| Noortman, 2019 | [Noortman, 2019] | 11.17 | 1968 | 555 total (~ 185 unit) |

## B.5 Choice of index building for URM3M_U

Figure B.6 presents the distribution of the properties of URM3M_U as defined in [Crowley et al. 2017] and obtained from the V5 exposure database [Arup 2017b]. In the figures, the properties of the index building and the buildings assigned to the typology are indicated by arrows. The figure shows that Koeriersterweg index building is representative for the gutter height and footprint area of the buildings within URM3M_U, while it might be older compared to the majority of the buildings in the typology. Rijksweg 107-117 appears to be on the higher-end for the gutter height, related to the small pitch of the roof (much smaller than Koeriersterweg). Overall it can be concluded that both building are representative of URM3M_U typology.

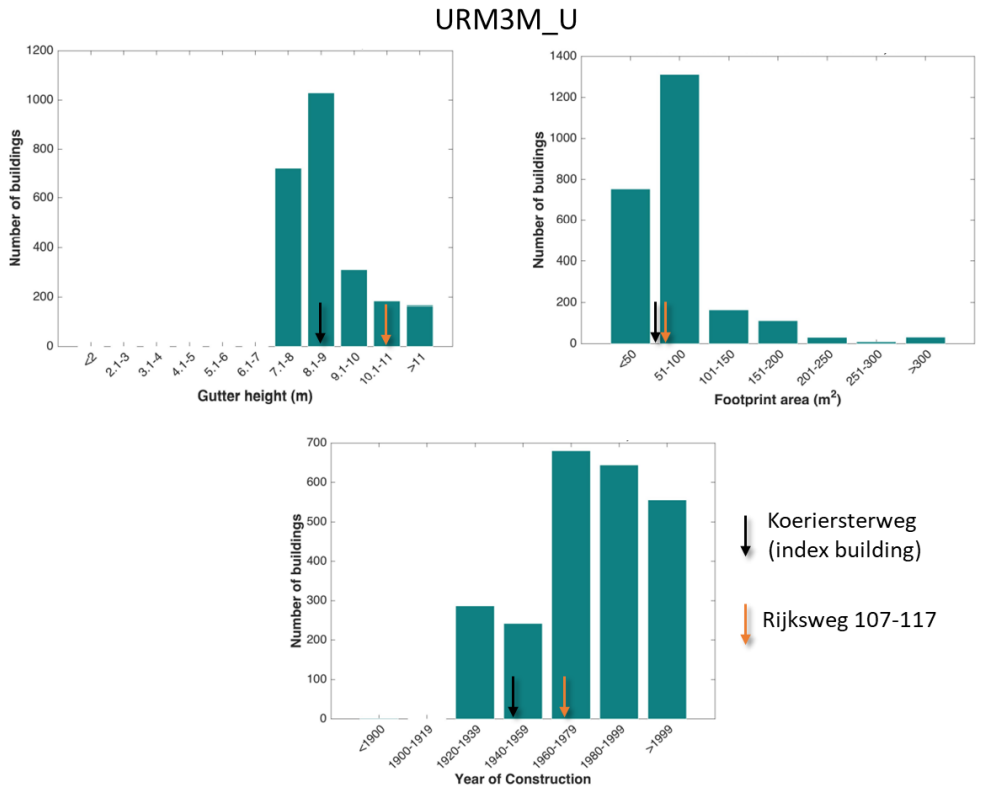


Figure B.6 Distribution of gutter height, footprint area and construction year of the buildings within URM3M_U adapted from [Crowley et al. 2017] and obtained from the EDB V5, [Arup 2017b]. The black arrow represents the index building of URM3M_B provided in [Crowley et al. 2020]. The other arrows represent the buildings that are most similar to the index building of URM3M_U.

## B.6 Choice of index building for URM3M_B

Figure B.7 presents the distribution of the properties of URM3M_B as defined in [Crowley et al. 2015] and obtained from the V5 exposure database [Arup 2017b]. In the figures, the properties of the index building and the buildings assigned to the typology are indicated by solid arrows. The dashed arrow shows the footprint area related to one unit of the building. From the figure it is concluded that Schuitenzandflat and “Noortman, 2019” are both representative for URM3M_B typology. The same conclusion was drawn in terms of seismic capacity in Appendix A.

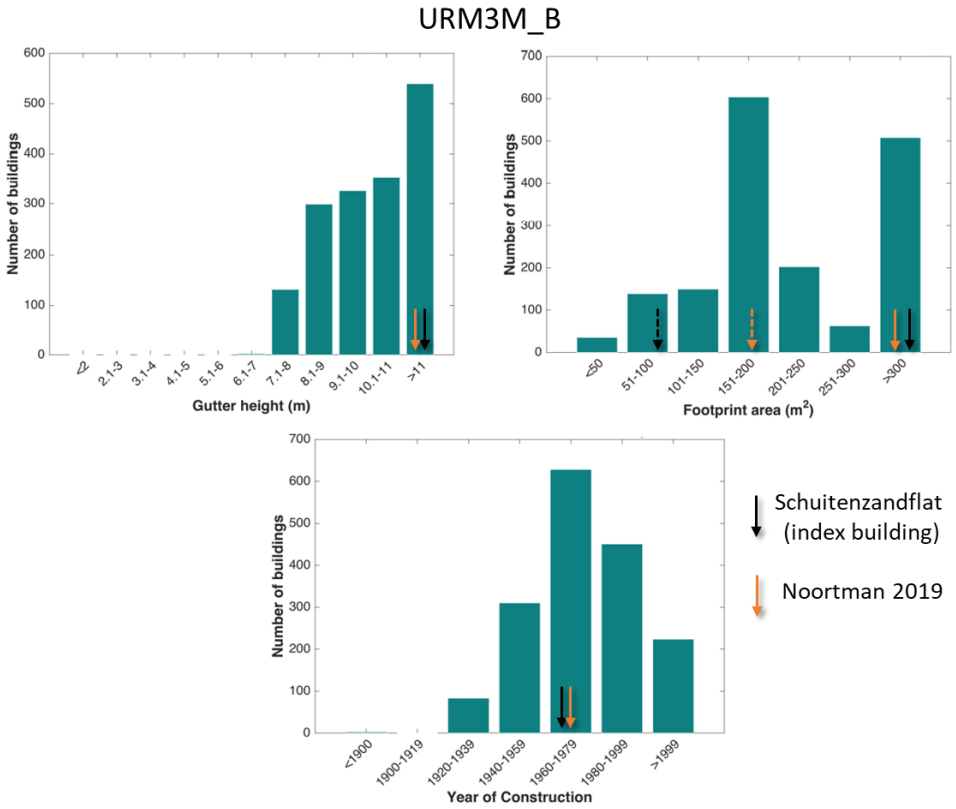


Figure B.7 Distribution of gutter height, footprint area and construction year of the buildings within URM3M_B adapted from [Crowley et al. 2017] and obtained from the EDB V5, [Arup 2017b]. The black arrows represent the index building of URM3M_B provided in [Crowley et al. 2020]. The other arrows represent the buildings that are most similar to the index building of URM3M_B. The dashed arrow shows the footprint area related one unit of the whole building.

## B.7 Conclusions

To establish fragility functions and compute a risk using a typology based approach, the building stock is divided into typologies and, for each typology, median buildings are selected as representative examples. The clustering process of the buildings is documented in the so-called exposure database (EDB) [Arup 2017b, 2019d] which also provides the distribution of the relevant properties of the buildings in each typology. The representativeness of the selected median buildings was investigated

for a different version of the fragility and consequence model developed by Eucentre, by comparing geometric properties and construction years of the index buildings to the distribution of the typology they represent (obtained from the EDB). The properties of the index buildings are reasonably representative of the respective typologies. Moreover, most of the relevant structural properties are already accounted for in the typology classification.

# C Summary of the material received from NCG

To increase the confidence in the fragility and consequence model proposed for METSELWERK-D, TNO has received assessments of buildings which could be potentially assigned to METSELWERK-D by the Nationaal Coördinator Groningen (NCG). The material received consisted of 28 Technical Strengthening Advices (Technisch Versterkings Advies, TVA). Each TVA contains multiple addresses. The material was first reviewed to select those buildings which comply with the description of METSELWERK-D: regular floor plan (rectangular), number of storeys between three and five, concrete floors and unreinforced masonry (URM) walls. From this selection, only buildings assessed using non-linear push-over (NLPO) or non-linear time-history (NLTHA) analyses have been selected. From such analyses, capacity curves in terms of base shear and attic displacement capacity can be derived and compared to the ones of the index buildings within METSELWERK-D.

The list of NCG addresses from which assessments were received are provided in Table C.1. The table indicates whether the building was compliant to METSELWERK-D and whether it was utilized or not for the comparison against the index buildings. From the 28 TVAs, 15 are compliant to METSELWERK-D.
From the excluded 13 TVAs, 7 involved buildings with less than three storeys, 5 have a non-rectangular plan shape, 1 has a concrete structure.
Out of the 15 TVAs, 6 are selected to be used for additional analyses and comparison against the index buildings. For 1 TVA only the analyses of the retrofitted building are available, so it is not suitable for comparison. The remaining 8 TVAs were excluded because these were evaluated using equivalent linear analysis.

Table C.1 Description of TVAs received from NCGs of buildings that could potentially be assigned to METSELWERK-D.

| NCG ID | # addresses of NCG ID | Number of TVAs | Analysis type | Number of stories | Rectangular shape | Remarks | Compliant to typology | Selected for analysis | Reference |
|---|---|---|---|---|---|---|---|---|---|
| APPD_AEPPEN_AG | 28 | 2 | MRS | 5 | Yes | Equivalent linear analysis | **Yes** | No | |
| APPD_AEPPEN_GF | 99 | 1 | NLTHA | 4 | Yes | | **Yes** | **Yes** | [Arup 2017c] |
| APPD_CALBRT_7-7D | 5 | 1 | NLTH | 2 | No | | No | No | |
| APPD_DERANK_AG | 10 | 1 | NLTH | 4 | Yes | | **Yes** | **Yes** | [Arup 2017e] |
| APPD_DPAASW_D3 | 27 | 1 | NLPO | 3 | Yes | Reinforced concrete structure | No | No | |
| APPD_GVSAKS_AG | 42 | 1 | NLTHA | 4 | yes | | **Yes** | **Yes** | [Arup 2017d] |
| APPD_GVSAKS_GF | 28 | 1 | MRS | 4 | Yes | Equivalent linear analysis | **Yes** | No | |
| APPD_HARKEN_AG | 30 | 1 | MRS | 4 | Yes | Equivalent linear analysis | **Yes** | No | |
| APPD_MBORGS_GF | 21 | 1 | MRS | 4 | Yes | Equivalent linear same analysis of APPD_AEPPEN_GF | **Yes** | No | |
| DELF_BALTICPK_AG | 48 | 1 | MRS | 5 | Yes | Equivalent linear analysis | **Yes** | No | |
| DELF_DEHELL_AG | 9 | 1 | NLPO | 4 | Yes | | **Yes** | **Yes** | [VIIA 2020] |
| DELF_EMSKNZ_AG | 27 | 1 | MRS | 5 | No | | No | No | |
| DELF_FINSST_GF | 84 | 1 | MRS | 5 | yes | Equivalent linear analysis | **Yes** | No | |
| DELF_MIDSCH_01 | 16 | 1 | NLTH | 5 | No | | No | No | |

| NCG ID | # addresses of NCG ID | Number of TVAs | Analysis type | Number of stories | Rectangular shape | Remarks | Compliant to typology | Selected for analysis | Reference |
|---|---|---|---|---|---|---|---|---|---|
| DELF_OUDSCH_AG | 15 | 1 | NLTH | 6 | No | | No | No | |
| DELF_RIJKSW_AG | 54 | 2 | NLPO | 4 | Yes | | **Yes** | **Yes** | [VIIA 2019a, 2019b] |
| DELF_SCHUIT_GF (1) | 84 | 1 | MRS | 5 | Yes | Equivalent linear analysis | **Yes** | No | |
| DELF_SCHUIT_GF (2) | 28 | 1 | NLTH | 5 | Yes | Only retrofitted building | **Yes** | **No** | |
| FARM_EEMSKZZ_18-22 | 29 | 1 | NLTHA | 7 | No | | No | No | |
| UITH_OUDTIL_23 | 1 | 1 | MRS | 1 | No | | No | No | |
| Not found –duplex (5B) TBOE_WEDMAN_DU | Not found | 1 | NLPO | 2 | Yes | | No | No | |
| Not found – duplex (5B) APG_Bouwmeesterstraat - Molenstraat | Not found | 1 | NLPO | 2 | No | | No | No | |
| Not found - kantoorgebouw (5C) 9919_AE_13 | Not found | 1 | MRSA | 1 | Yes | | No | No | |
| Not found - MKB pand (5D) APPD_SOLWRD_32 | Not found | 1 | MRS | 2 | No | | No | No | |
| Not found - MKB pand (5D) APPD_STANNA | Not found | 1 | NLTH | 2 | No | | No | No | |
| Not found - MKB pand (5D) | Not found | 1 | NLTH | 5 | No | | No | No | |